SHOCK TUBE DESIGN AND THE KINEMATICS OF THE HYBRID III DUMMY HEAD UNDER SHOCK WAVES OF BLAST

A Thesis
Submitted to the Graduate Faculty
Of the
North Dakota State University
Of Agriculture and Applied Science

By

Ka-Ho Derek Leung

In Partial Fulfillment of the Requirements
For the Degree of
MASTER OF SCIENCE

Major Department:
Mechanical Engineering

April 2012

Fargo, North Dakota

North Dakota State University

Graduate School

Title

Shock Tube Design and the Kinematics of the Hybrid III Dummy Head under Shock Waves of Blast

By

Ka-Ho Derek Leung

The Supervisory Committee certifies that this ***disquisition*** complies with North Dakota State University's regulations and meets the accepted standards for the degree of

MASTER OF SCIENCE

SUPERVISORY COMMITTEE:

Dr. Ghodrat Karami
Chair

Dr. Mariusz Ziejewski

Dr. Fardad Azarmi

Dr. Benton Duncan

Approved:

April 2012

Dr. Alan Kallmeyer
Department Chair

ABSTRACT

Traumatic brain injury (TBI) is one of the most common injuries to soldiers in warfare today. A TBI occurs when the human brain is damaged by a sudden force coming from the environment. Blasts created by improvised explosive devices (IEDs) can cause damage to other human body parts including lungs, bowels, and any other air-containing organs. In this study, a blast shock tube was constructed for use with a Hybrid III dummy head model for mimicking the blasting scenario to obtain mechanical behavior data from when the generated compressed air is released from the blast shock tube. The acceleration based on the standoff distance of the Hybrid III head could be found. A simple model was established for finite element (FE) analysis. The results showed that the closer the dummy head was to the shock tube opening and the higher the pressure pulse being used and more.

ACKNOWLEDGEMENTS

I would like to thank my advisors, Dr. Ghodrat Karami and Dr. Mariusz Ziejewski, for supporting and guiding me through my Master's Degree program. I would also like to thank Dr. Fardad Azarmi and Dr. Benton Duncan for serving as the Supervisory Committee Members for my research, Dr. Majura Selekwa for his support on the data acquisition system setup and a special thanks to my colleagues for their help, support, and recommendations leading to the completion of this research.

The research was supported financially by the U.S. Army; therefore I would also like to thank the United States Army for financially supporting the research, and the Mechanical Engineering Department, North Dakota State University for providing me with financial support during the time that I was in the Master's Degree program. Finally, I want to thank my family and my friends for encouraging me, and lifting me up every time I had any type of difficulties.

TABLE OF CONTENTS

LIST OF TABLES

LIST OF FIGURES

CHAPTER 1. INTRODUCTION AND RESEARCH OBJECTIVES

In the field of combat, high pressure blasts created by improvised explosive devices (IEDs) are always a threat and are the major cause of traumatic brain injuries (TBIs). Therefore traumatic brain injuries caused by IEDs are called 'signature wounds' of any wars today (Magnuson, 2010).

TBI is one of the most common injuries happening to soldiers today, and research on diagnosing TBIs is one of the major components for determining treatments for them, as well as means for preventing them. TBI occurs when a human brain is hit by a sudden force, acceleration, or deceleration coming from the environment. Acceleration is the most important engineering parameter that leads to brain injury, as it shows the change of velocity depending on time. As a result, the severity of the brain injury is characterized based on the acceleration of the human head, while the acceleration is determined by the combination of three linear acceleration components and three angular acceleration components (Ziejewski et al., 2007).

According to the Department of Veterans Affairs in 2007, there were about 1800 troops with TBIs. Neurologists have estimated that roughly 30 percent of the troops that are at risk to TBI may also be at high risk to get any type of neurological disorder after four months or longer of combat, due to the blast conditions coming from the explosives (Glasser, 2007).

It is estimated that 19.5% of all U.S. troops have symptoms related to blast induced traumatic brain injury (bTBI), which is possibly the cause of the neurological disorders like migraine headaches, insomnia, or dizziness (Helmick et al., 2006, Tanielian & Jaycox, 2008, Anderson, 2008, Cifu et al., 2009)

1.1. Explosive Materials

Explosives are one of the most common weapons used in warfare today. They are extremely dangerous due to their explosions and blast radius. A description of the mechanism of the explosive is that it is simply the energy of motion. For example, the explosive consisting of trinitrotoluene (TNT), with proper handlers, is an object that has chemical potential energy. When the TNT is detonated, the potential energy is turned into kinetic energy and motion is created. At the same time, blast is formed when the motion of air starts. Other than the blast, thermal energy is created due to the blast, which involves a high velocity change of the air. Such a process is considered to be exothermic, which is an energy releasing reaction from the system. Most of the time, this process is in the form of heat, light, or sound (WebRef3, 2012).

The explosives are classified as low-order and high-order. The low-order explosives create explosions that are supposedly slower than Mach 1, which is the speed of sound. The low-order explosives produce a subsonic wave, and the high-order explosives produce a supersonic wave, which is an over-pressurization wave that the low-order explosives would never have (WebRef3, 2012).

In the battle field, military purposed explosives are all high-order explosives, while the terrorists would use high-order explosives, low-order explosives, or the combination of both (WebRef3, 2012).

1.2. Blast Injuries Classification

Blast injuries can be classified into the four major mechanisms of primary, secondary, tertiary, and quaternary. The blast injuries classifications are based on the anatomical and physiological changes from the body being impacted by any external forces (WebRef2, 2012).

Primary blast injuries are caused by the impact of the shock wave to our human bodies. In other words, the injuries are caused when human body is being hit by the blast that changes the atmospheric pressure of any medium (Ziejewski et al., 2007), and may occur without any visible external signs. These Injuries mostly occur in specific organs that contain air, such as lungs and bowels. Other than those organs, it is believed that the shock wave can also damage the human brain (Brooks et al., 1997).

Secondary blast injuries are caused by the impact of fragments and any objects within the bombing device that are accelerated by the blast. Injuries in this classification can be categorized as penetrating or non-penetrating, depending on the injuries (Brooks et al., 1997).

Tertiary blast injuries are caused by the sudden acceleration of the human body by the blast which then hits the ground or any rigid objects leading to any tearing of body parts or tissue (Brooks et al., 1997). The fourth type of blast injuries mechanism is the quaternary, which are related to burns due to the

explosion, the combustion of the environment, or any dangerous gas that is not related to any of the other three classifications of blast injuries (Brooks et al., 1997). The following is a table of mechanisms for the blast injury.

Category	Characteristics	Body Part Affected	Types of Injuries
Primary	Unique to HE, results from the impact of the over-pressurization wave with body surfaces.	Gas filled structures are most susceptible – lungs, GI tract, and middle ear.	Blast lung (pulmonary barotraumas) TM rupture and middle ear damage Abdominal hemorrhage and perforation – Globe (eye) rupture – Concussion (TBI without physical signs of head injury)
Secondary	Results from flying debris and bomb fragments.	Any body part may be affected.	Penetrating ballistic (fragmentation) or blunt injuries Eye penetration (can be occult)
Tertiary	Results from individuals being thrown by the blast wind.	Any body part may be affected.	Fracture and traumatic amputation Closed and open brain injury
Quaternary	All explosion-related injuries, illnesses, or diseases not due to primary, secondary, or tertiary mechanisms. Includes exacerbation or complications of existing conditions.	Any body part may be affected.	Burns (flash, partial, and full thickness) Crush injuries Closed and open brain injury Asthma, COPD, or other breathing problems from dust, smoke, or toxic fumes Angina Hyperglycemia, hypertension

Table 1-1: Mechanisms of Blast Injury (WebRef2, 2012).

Based on the level of pressure of the blast, it causes different kinds damage to the human body. The following is a brief table showing the damage caused by different levels of blast overpressure (Kinney and Graham, 1985).

Type of damage	Overpressure (psi)
Personnel knocked down	~1-1.5
Eardrum rupture	~5-15
Lung damage	~29-75
Lethality	~100-220

Table 1-2: Correlation between damage and overpressure (Kinney and Graham, 1985).

1.3. Blast Conditions

A blast can be created by using several methods. One method would be to create an explosive, and another common method would be to construct a shock tube, which involves the work of compressed gas. In the battlefield, blasts are found mostly by the detonation of the explosive materials. The strength of the blast caused by the explosive materials depending on two major elements. One of the two elements is the explosive charge weight, which is measured based on the identical amount of TNT. The other element is the standoff distance between the explosive and the object that is receiving the blast that is created by the explosive (Ziejewski et al., 2007).

A shock tube would be a better or safer way to create shock waves versus making an explosive, which would be more dangerous. There are two main sections of a shock tube: 1) the driver section and 2) the driven section. The

high pressure gas is usually stored in the driver section of the shock tube while the driven section usually contains low pressure gas, or ambient environment. The two sections are separated by a component, which can be a rupture disk or a butterfly valve that can be opened quickly, depending on the preference.

As the separating component is gone or opened quickly, the high pressure gas in the driver section flows into the driven section. Such operation finally creates the blast condition as the gas in the driver section is going into the driven section with an extremely high velocity. The high pressure gas ends up having the same pressure as the low pressure gas after a short period of time.

The driven section can sometimes be called the chamber section, because there is usually a test chamber in the section. Testing devices can be placed in the chamber section so data can be obtained by performing the test. Some examples of these testing devices would be any load cells, accelerometers, air velocity transducers, pressure sensors or any other devices.

After the explosion occurs, a high pressure is formed in an extremely short period of time. After that, the high pressure generated from the explosion travels outward as a wave with an extremely high velocity. The high pressure was then lowered quickly due to the surrounding condition, and finally returned back to its normal condition. This was the process of the shock wave, as shown as Figure 1-1 (Brooks et al., 1997).

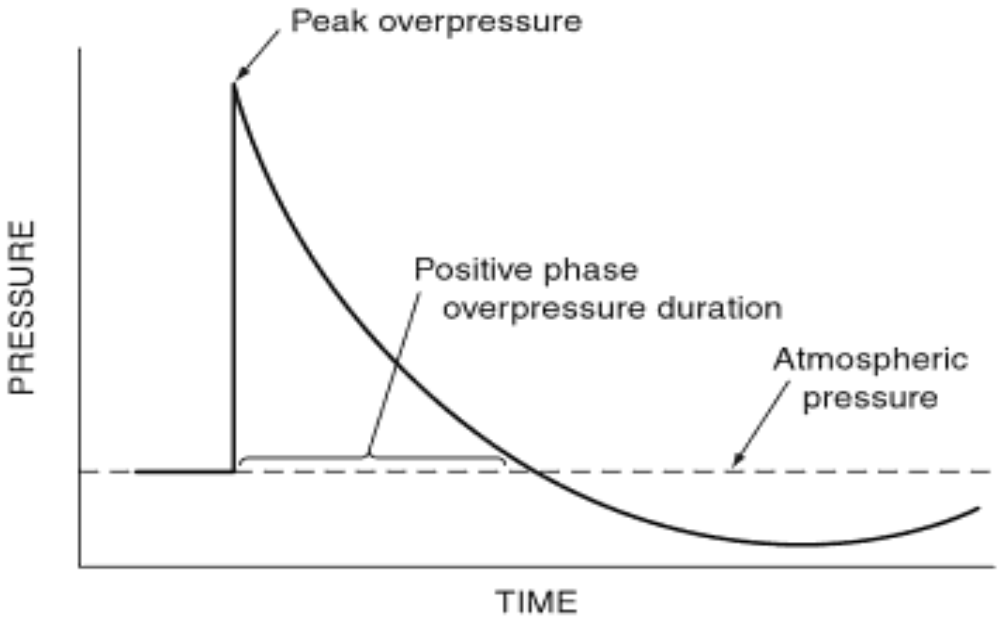

Figure 1-1: A classic Pressure vs. Time curve at a point at the scene (Brooks et al., 1997).

The pressure distribution curve based on time can be determined by using the following equation.

$$p(t) = p_0 + p_s^+ \left(1 - \frac{t}{T^+}\right) e^{\frac{-t}{T^+}} \quad (1\text{-}1)$$

where p_0 is the atmospheric pressure, p_s^+ is the peak overpressure, t is the time when the pressure starts to shoot up, T^+ is the time duration for the positive phase.

The peak overpressure drops gradually and slowly as the shock wave travels outward from the explosion point. Figure 1-2 shows the relationship between the peak overpressure and the distance away from the explosion site with an assumption of 10 kg of trinitrotoluene being used as an explosion (Brooks et al., 1997).

Described as a danger to the human body, a powerful explosive would generate blast waves of high pressure at a velocity of about 1600 ft/s from the explosive and with a radius of a few hundred yards. The blast wave has two different parts that cause damage to the human body: 1) the wave that causes the positive phase overpressure, 2) after the first wave, as the air or any medium is being forced hard, the vacuum space is created. The vacuum space is then filled up with air and this causes high pressure again, which represents the negative phase of overpressure. These sudden changes of pressure are leading to the neurological injury, as traumatic brain injury would be part of (Glasser, 2007).

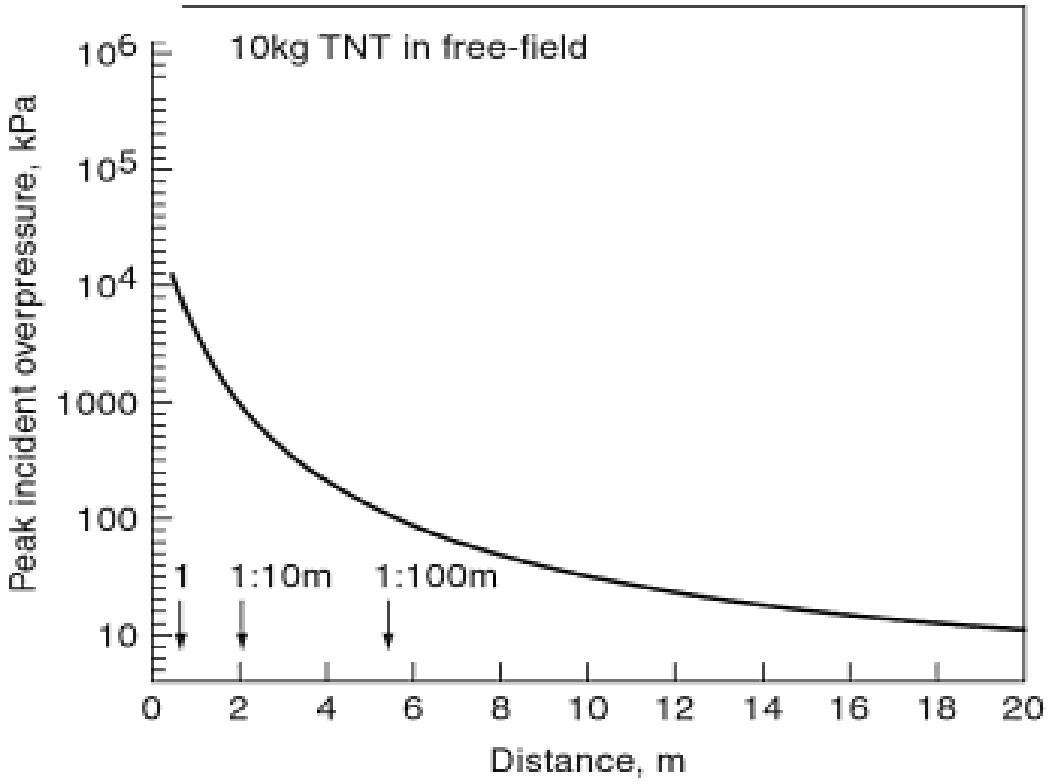

Figure 1-2: The relationship between peak overpressure and standoff distance when 10 kg of TNT is being used (Brooks et al., 1997).

1.4. Traumatic Brain Injury

This study is related to TBIs caused by primary blasts. Recently, there has been an increasing amount of research on TBIs as they are still a major concern for the U.S. Army branches. A TBI occurs when a blast wave hits a human head, causing a sudden acceleration of the head, leading to the brain responding separately to the sudden environment as the skull and the brain have different material properties. Brain tissues are first compressed then impacted against the skull and the brain tissues expand/compress over and over again inside the skull, and such movement causes void and destruction to the brain tissues (Ziejewski et al., 2007).

According to the National Institute of Neurological Disorders and Stroke (NINDS), a person with a mild Traumatic Brain Injury (mTBI) may remain conscious, or lose consciousness for a few seconds to minutes. Besides losing consciousness, other symptoms of mTBI include confusion, dizziness, and blurred vision. When a person has a moderate, or severe TBI, he/she may experience the same symptoms as a mTBI, but also seizures, loss of coordination, agitation and more (WebRef4, 2012). Besides injuring human heads, TBIs also have a negative impact on the economy. In just the year 2000, TBIs cost the U.S. national economy about 60 billion dollars (Finkelstein and Corso et al., 2006), while the National Centers for Disease Control and Prevention (CDC) estimated a cost of about 76.5 billion dollars in 2000 which included the direct medical costs and the indirect costs such as lost of productivity in 2000.

1.5 Research Objectives

The objective of this research was to determine the motion of the Hybrid III Dummy Head when it is hit by the pressure pulse generated by the blast shock tube. This research is divided into three major parts.

The first part of the research was the construction of a blast shock tube and the stands along with a rail system for the dummy head. The shock tube was used to simulate the blast similar to the blast condition created by the explosions of explosive materials. The assembling of stands and rail system for the dummy head was for the purpose of allowing the dummy head to slide through in a uni-direction when being hit by the pressure pulse generated by the blast shock tube.

The second part of the work was to measure the linear velocity and acceleration of the Hybrid III Dummy Head when it was subjected to various pressure pulses generated by the shock tube. The measurement of the velocity and acceleration of the dummy head was to determine the damage that the dummy head might experience, as a TBI is caused by the sudden acceleration of a human head.

The third part of this research was to determine the relationships between the linear velocity, acceleration of the head model and the pressure pulse using finite element (FE) analysis, as well as the relationship between the pressure pulse and the standoff distance. The FE analysis approach helped in understanding the mechanism of the blast on the head model that was similar to the experiments. The use of FE analysis software could have also helped determine the reaction of the air flowing inside the chamber section of the shock tube.

CHAPTER 2. A REVIEW OF BLAST SIMULATION BY SHOCK TUBE AND NUMERICAL COMPUTATION

This chapter describes some past studies that are related to this research. Some of the studies are about the construction of the shock tube, while others involve the reactions that have occurred in rat brains under a blast, or how the pressure has changed in a specific area inside the shock tube over a period of time. Other than experimental research, numerical research has also been conducted by using head models for simulating the reactions to the human head. These studies had some reasonable results and are therefore useful references for other researchers.

2.1. Blast Simulation Experiments

The shock tube constructed by Ronald Segars and Marina Carboni at the U.S. Army Natick Soldier Research Development and Engineering Center (NSRDEC) showed important data on the differences when assorted test materials were used (Segars et al., 2008). The testing materials for their research include three different types of foams, Kevlar ® fabric, and aluminum foil while all had different material properties. The shock tube was made of stainless steel pipe with an inner diameter of 6.72 cm and an outer diameter of 7.28 cm, respectively. The driver section of the tube was 30.5 cm long while the driven section was exactly 183 cm long. For each section of both, there were two stainless steel flanges attached to each end. The yield strength of the used tube was about 4000 psi, which was close to the pressure that the tube could

hold. There was also a total of five sensor taps used on the shock tube, for finding the changes of the pressure at different spots inside the shock tube. Placing multiple pressure sensors at different sections in the shock tube give out different pressure distributions of the flow. Figure 2-1 shows a set of plots with data obtained from the four pressure taps, P1 is for the flow in the tube wall by the diaphragm, P2 is in the tube wall by the endplate, P3 measures the reflected pressure at the endplate, and P4 measures the reflected pressure at the recessed sensor.

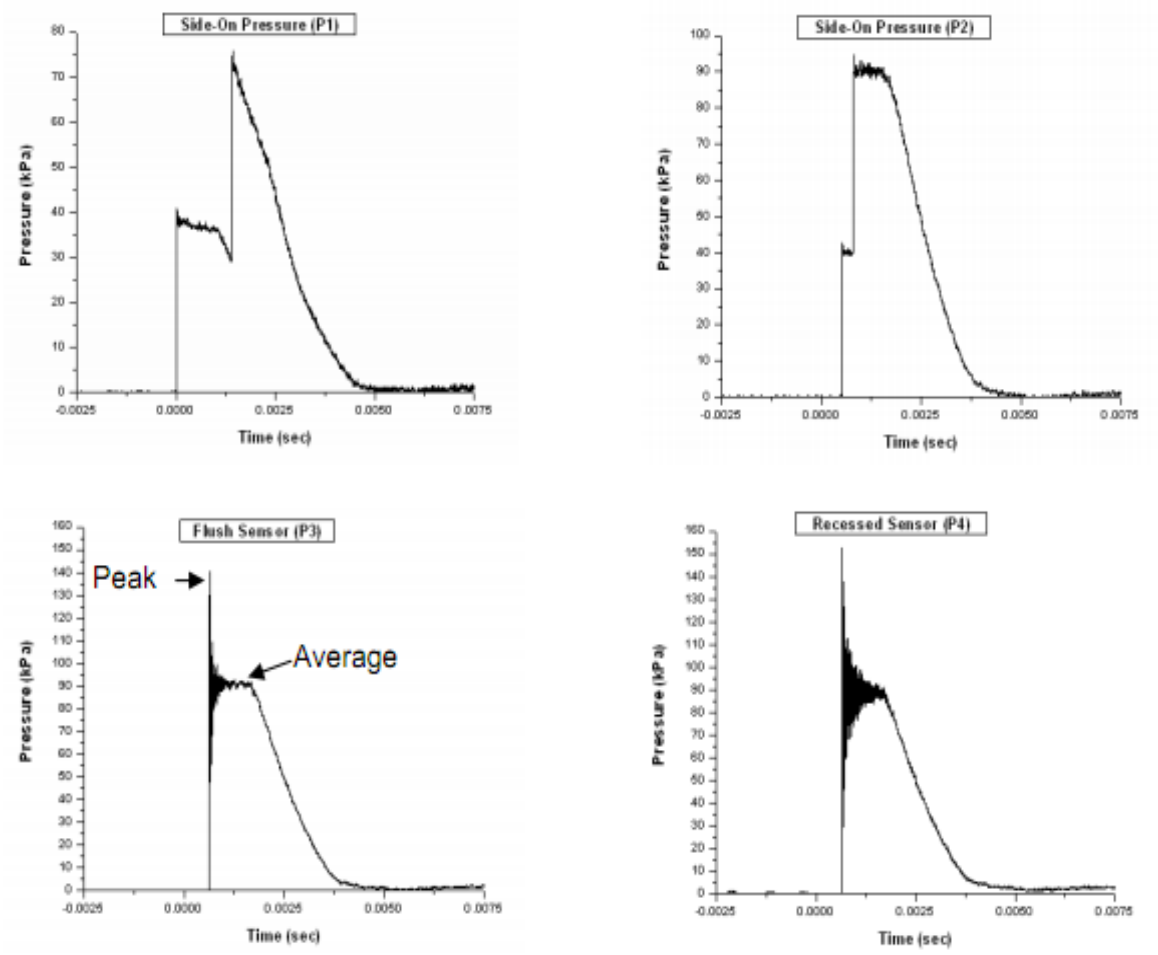

Figure 2-1: Pressure distributions at different locations in the shock tube (Segars et al., 2008).

A shock tube made by Leonardi et al. (2011) was used at Wayne State University (WSU) to study the increases of intracranial pressure (ICP) due to shockwaves. The shock waves were generated by using helium as the driven gas, the shock tube had a total length of 272 inches, which included the 30 inches driver section and the 242 inches long driven section. To verify the accuracy of the results in the case of using the in vivo method, 25 male Sprague-Dawley rats were used in the experiment while guided cannula was placed inside the rats' skulls. The rats were then placed in a soft hold inside the shock tube so they would face the shockwaves once the test is run. Unlike the other shock tubes, the one at WSU had a transparent pipe at one end of the metal pipe. The purpose of the transparent pipe was to make the full process of the experiment visible, by human vision. By using a high speed camera, the researchers did not have to stand by the opening of the shock tube. Similar to the other shock tube experiments, this shock tube helped obtain the data of ICP over a short period of time. There was a possibility that the ICP could change due to how the cannula was sealed, Leonardi et al. (2011) tried different scenarios when the cannula was unsealed, partially sealed, or fully sealed. Figure 2-2 shows the difference between the different situations.

The results show that the incident shockwave overpressure had the lowest peak overpressure while the totally sealed cannula had the highest peak overpressure. Overall, the pressure was the highest when the cannula was partially sealed. Negative pressure occurred for all the cases when the time got to roughly 18.5 ms.

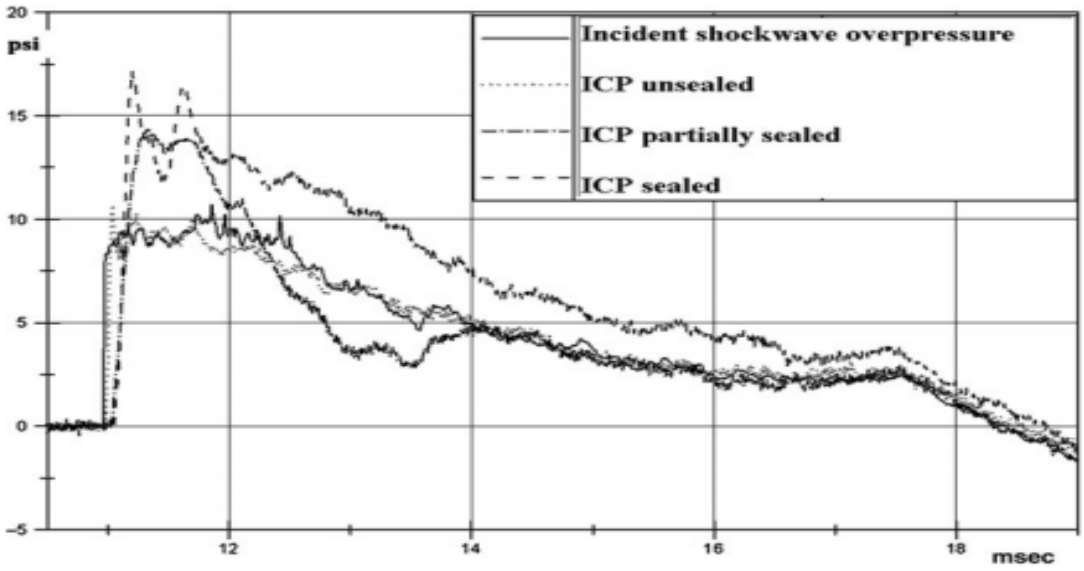

Figure 2-2: Results based on different situations (Leonardi et al., 2011).

2.2. Finite Element Analysis Simulations

FE analysis is a powerful tool for studying air blast and TBIs. Yet the accuracy of the results from these simulations is highly dependent on the accuracy of the model (Chafi et al., 2010). This includes material properties for different parts of the model, geometry of the model, and conditions related to the situation of the scene. Finite element analysis (FEA) can be used to analyze the stress and displacement of the head model by using LS-DYNA. It can also help in determining the reaction of the air flow, the air flow velocity, or the stagnation pressure by using computational fluid dynamics (CFD).

A simple blast model usually involves the use of Arbitrary Lagrangian Eulerian (ALE) elements for the explosive/TNT charger and the surrounding environment/air while the detonation of the TNT is defined by using the Jones-

Wilkins-Lee (JWL) equation of state (EOS). The parameters for that specific equation were estimated by Dobratz in 1985.

$$p = A\left(1 - \frac{\omega}{R_1 V}\right)e^{-R_1 V} + B\left(1 - \frac{\omega}{R_2 V}\right)e^{-R_2 V} + \frac{\omega E}{V} \quad (2)$$

$$V = \frac{\rho_0}{\rho} \quad (3)$$

where p is the pressure, ρ_0 is the initial density of TNT, ρ is the density of the detonation gas, *A, B, R1, R2, ω* are the parameters for the JWL equation, and *E* represents the internal energy of the detonation.

A recent research on shockwave hitting on a sandwich panel by using the finite element method (FEM) was done by Tan et al. (2010). The objective of their research was to determine the performances of sandwich circular panels when different materials are used under the condition of blasting. The performances of the sandwiches were compared to performances found by using the monolithic solid circular plates. Finding that the results of the peak transmitted overpressure, deflection of the panels, and the acceleration of the sandwiches were less than the results for the monolithic solid plates. The research showed that the performance of the materials on the shock tube blasting condition was based on the material property, configuration, and mass distribution. Figure 2-3 shows a cross-sectional sketch of a shock tube for the sandwich panel experiment (Tan et al., 2010).

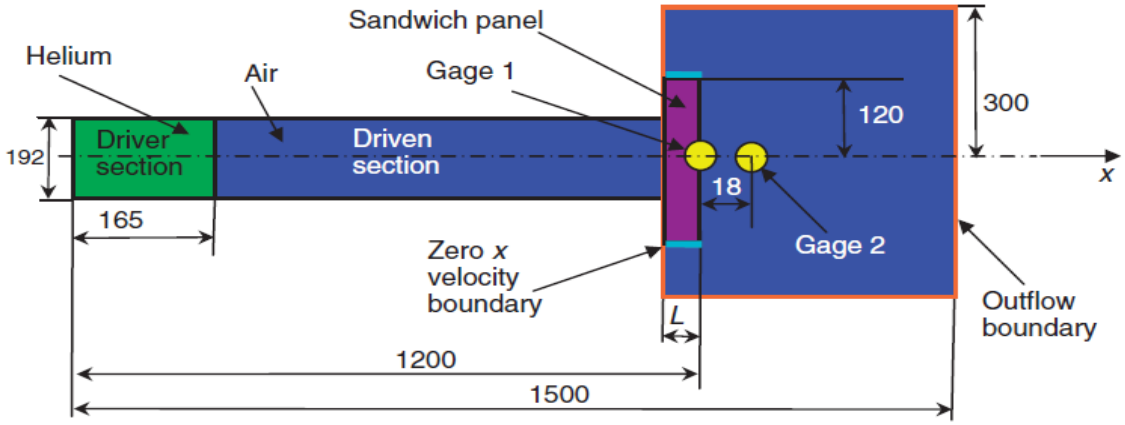

Figure 2-3: The 2D model of shock tube for the sandwich panel experiment (Tan et al., 2010).

By using such a model, with a boundary condition of 10 MPa applied to the driver section, the results generated by simulating the blast were obtained. Results could then be compared to the results obtained by using ConWep (Tan et al., 2010), which is a software developed by the US Army Corps of Engineers' Engineer Research and Development Center, which is shown as Figure 2-4.

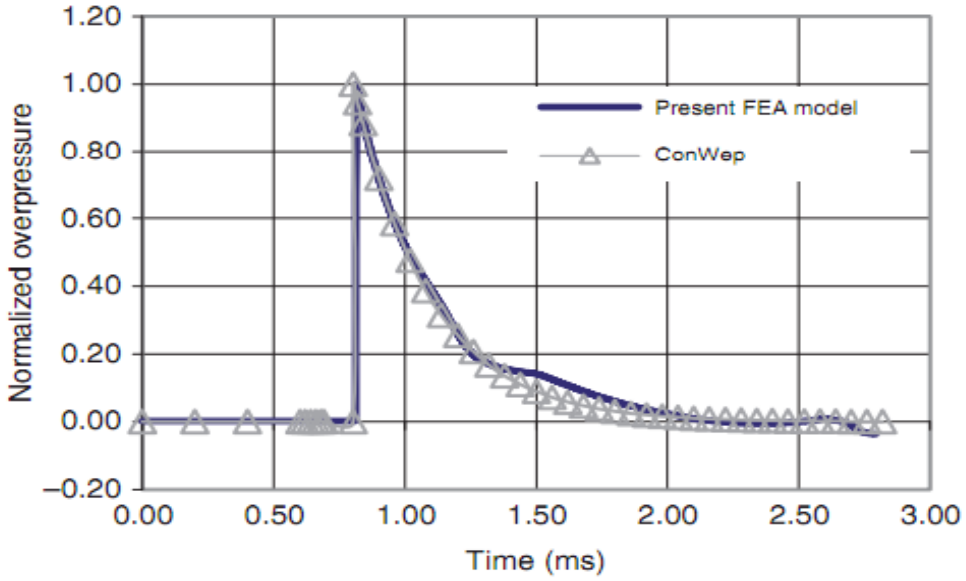

Figure 2-4: Comparison between FEA results and ConWeb (Tan et al., 2010).

To increase the accuracy of the modeling results, there were some modifications done to the previous model. Sandwich models were added to this model so the results could be compared to the results obtained from performing the chamber test. In this research, sandwich panels were made up of a combination of aluminum, polyethylene, Kevlar or nylon with SSP-core A or MSP-core B. Figure 2-5 shows the effect of the blast wave to the panel. The results show that the sandwich panels were more efficient than the solid panels.

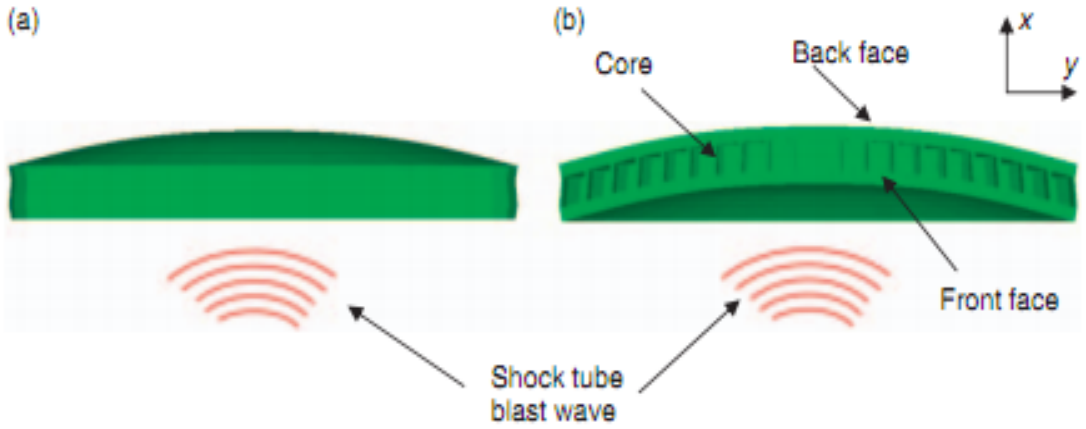

Figure 2-5: Different views on panel's deformation due to the blast as a) side view b) front view of the sandwich (Tan et al., 2010).

To determine any response of a human head and its relative motion by using FEA, high accuracies of dimensions and geometries of the human head and brain are not enough. There should also be some realistic boundary conditions and interface (Chafi et al., 2010). To simulate the blast-induced wave propagation by using LS-DYNA, a dynamic software, it was suggested to use two formulations, which were Arbitrary Lagrangian Eulerian (ALE) and Fluid-Structure Interaction (FSI) (Chafi et al., 2009). In the paper, the air blast model was

simulated by using multi-material ALE formulation as the ALE formulation. It was also determined the effects from an actual explosive, because each element of the model is to contain more than two different materials. FSI was to be simulated for the interaction of some moving or fixed mesh using an ALE formulation while the Lagrangian formulation was used for a deformable structure. The air blast simulations were conducted by using LS-DYNA with the usage of Eulerian Multi-Material, ALE formulations for the Navier-Stokes equations and the Jones-Wilkins-Lee equation for the results of the explosion. In the paper, the explosives used for simulations were C-4 and TNT and were simulated in an open space so that it could simulate a battlefield scene. The model is shown as Figure 2-6. The results for the simulation when C-4 explosives were used are plotted and compared to an experimental result obtained by Boyer (1960). The plot shows that the results were comparable and errors of the arrival time and peak pressure could be neglected.

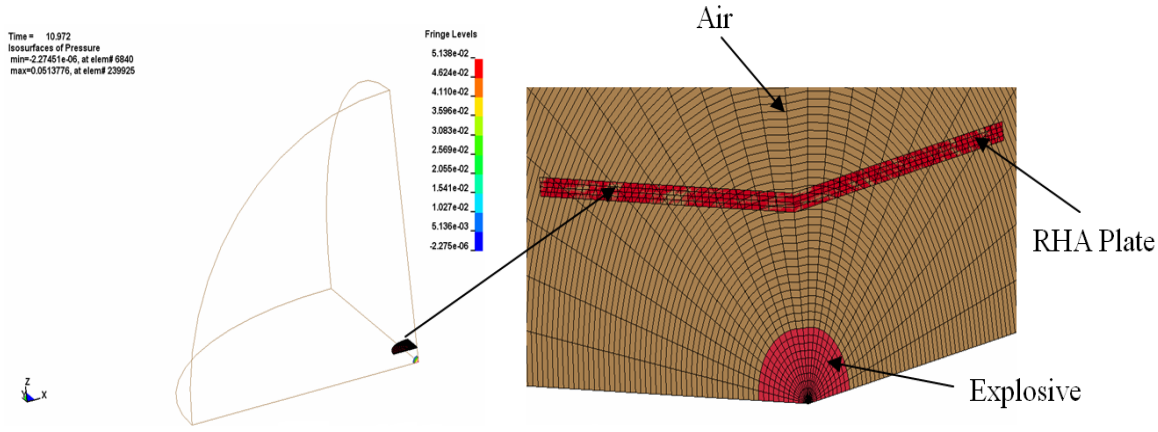

Figure 2-6: Meshed model consists of explosive, air, and rolled homogeneous armor plate (Chafi et al., 2009).

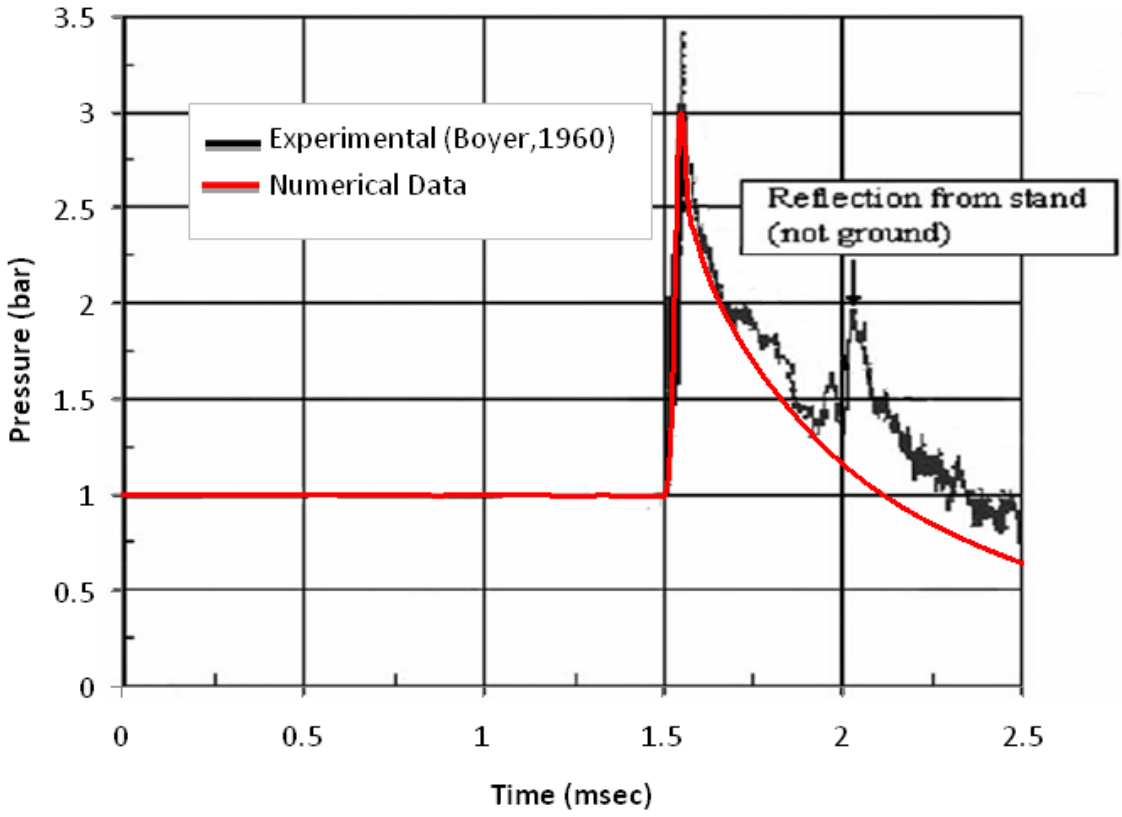

Figure 2-7: Comparison between the experiment result (Boyer, 1960) and the numerical result (Chafi et al., 2009).

After plotting the pressure distribution over time when C-4 was used, another chart was plotted for the result obtained when TNT was used. The chart shows the relationship between pressure and the distance from the explosion as the experimental result is gathered from another experiment, which was done by Gibson in 1994 (Chafi et al., 2009).

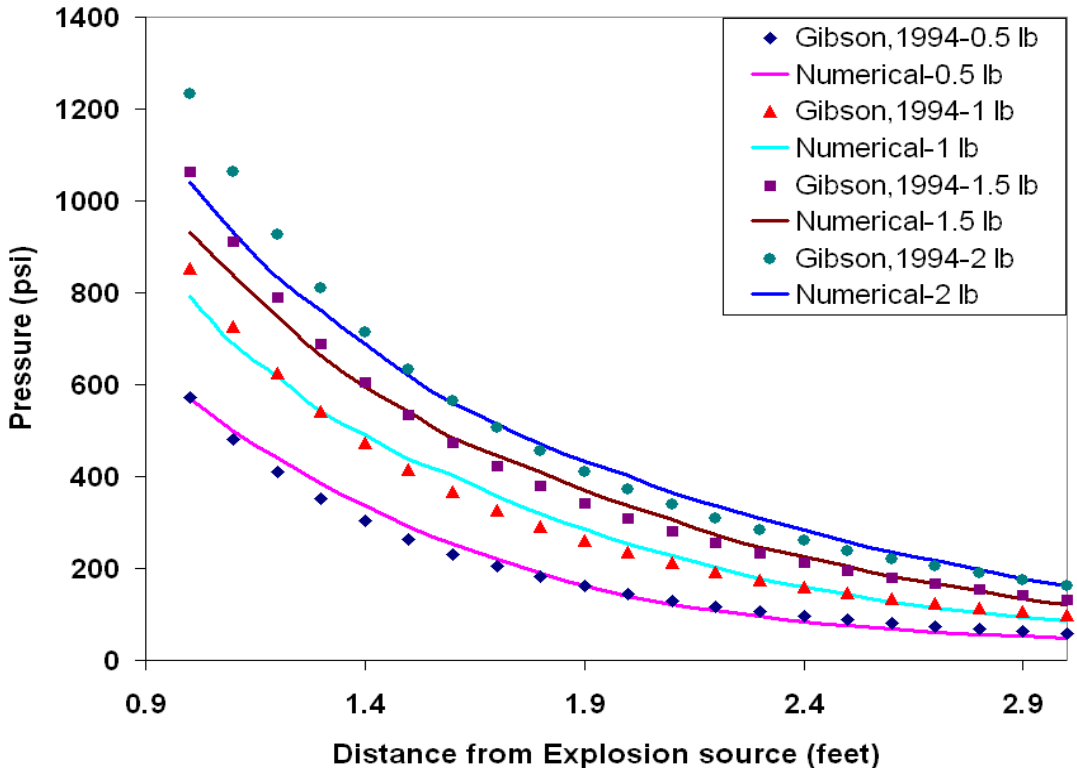

Figure 2-8: Pressure distribution based on distance from explosion while different amounts of TNT are being used (Chafi et al., 2009).

The results show that as the distance from the explosion became greater, the pressure got lower. The errors between the experimental results (Gibson, 1994) and the numerical results (Chafi et al., 2009) less than 10% when 0.5, 1, 1.5, 2 pounds of TNT explosives were being used. This indicated that the cases were in good agreements.

One research study was to assess the brain dynamic response when being hit by blast pressure waves with the use of FEA. The 3-dimensional (3-D) FE model was based on a highly detailed structure of a human head, which included the human brain, falx and tentorium, dura mater, cerebrospinal fluid

(CSF), scalp, skull bone, and pia mater. The following figure shows the particular 3-D FE model for the human head.

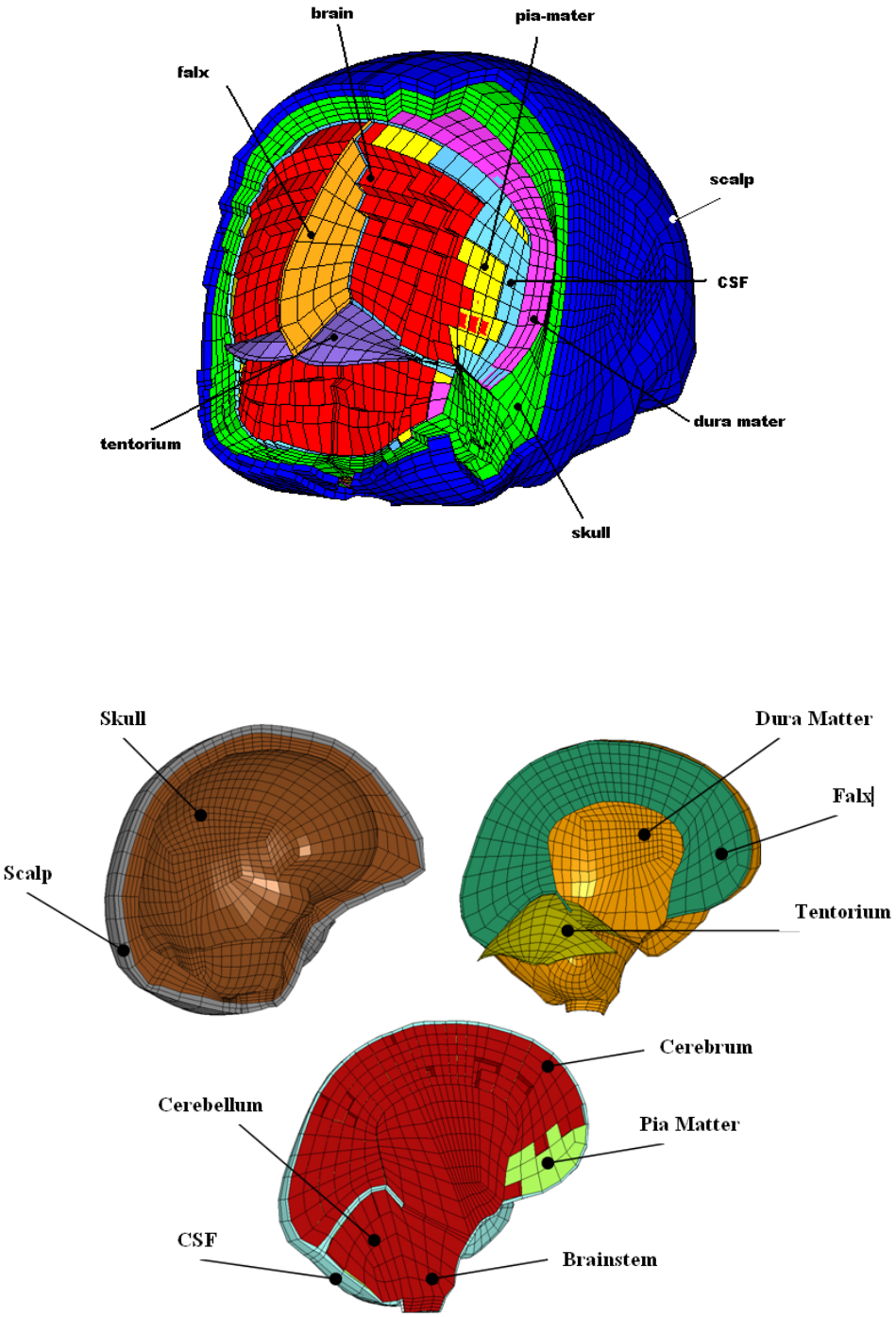

Figure 2-9: Different views of the head model showing different parts of the human head (Chafi et al., 2010).

In a paper by Chafi (2010), the CSF was normally clear fluid that acted as a cushion as it help protecting the brain and spine from injury and was modeled with solid elements along with fluid-like property. The interface between the dura and tentorium and the falx was defined to have a contact of tied node-to-surface as these particular parts are physically attached to each other in human head. In addition, the interface between the brain and membrane was modeled to have a tied contact algorithm as loads could be transferred in both compression and tension (Chafi et al., 2010). After modeling of the head, it used in the air-blast simulation using the multi-material formulation used in the previous paper (Chafi et al., 2009). In that case, the detonation was based on the explosion of high explosives (HEs).

From the simulation, ICPs, maximum shear strains, and maximum shear stresses were found through the time when the head human was hit by the blast and the shock waves. The simulation was conducted several times which included different amounts of the same explosive material. As expected, when the amount of explosive material used, the higher the pressure, shear stresses, and shear strain that occurred to the head model. The results showed that the response happened to the head and lasted for about five miloseconds for such blast impact. The following figure (Figure 2-10) shows the contour plot of pressure distribution of the air at different time since the detonation of an explosive, and a figure (Figure 2-11) showing the pressure reaction over time.

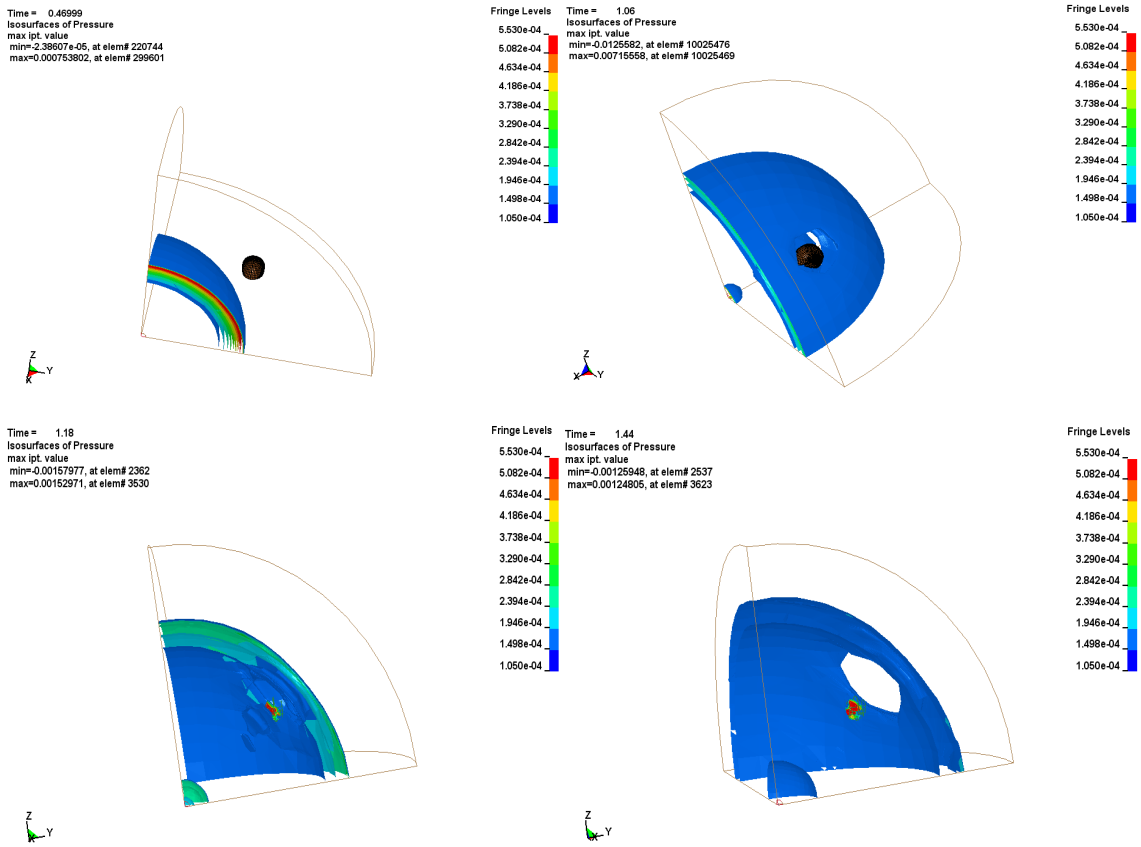

Figure 2-10: Pressure distribution of the model at different time (Chafi et al., 2010).

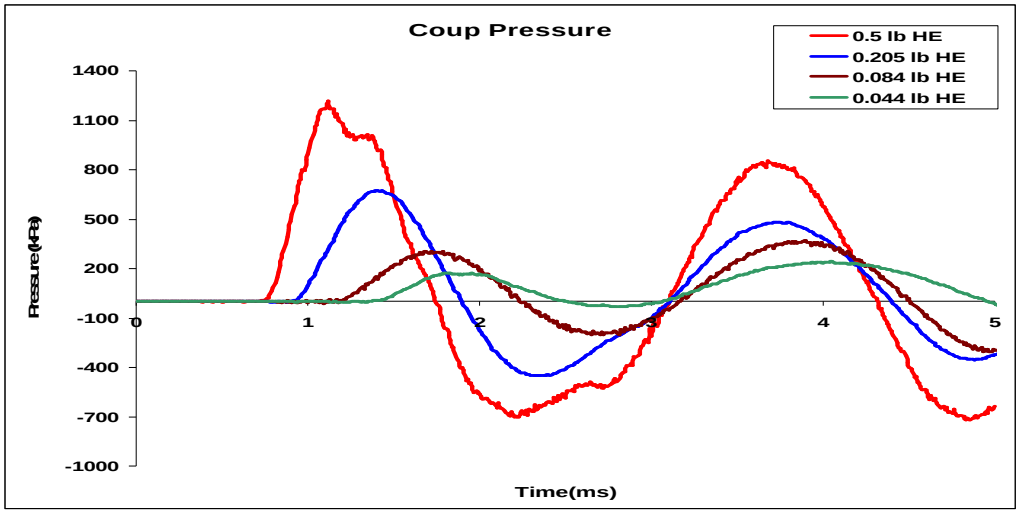

Figure 2-11: Average ICP over time when three different amounts of HEs are used (Chafi et al., 2010).

In the work of Dirisala et al. (2011), an FE head model that cosisted of almost all the parts of a human head was used. The geometry of the FE human head model was based on magnetic resonance imaging (MRI) data with a total of 28,816 nodes and 19,589 8-node brick elements along with 5344 4-node shell elements. The neck was created by using viscoelastic material by using discrete elements while different damping coefficients were used to determine the differences between each case. One end of the neck was assumed to be connected to the head model while the other end was constrained. The specific model is shown below. For the interfaces between the membranes in the head model, node-to-surface and surface-to-surface tied based contact was used for the simulations. The CSF was once again modeled to have some fluid-like properties. The CSF and membranes used tied contact (Dirisala et al., 2011).

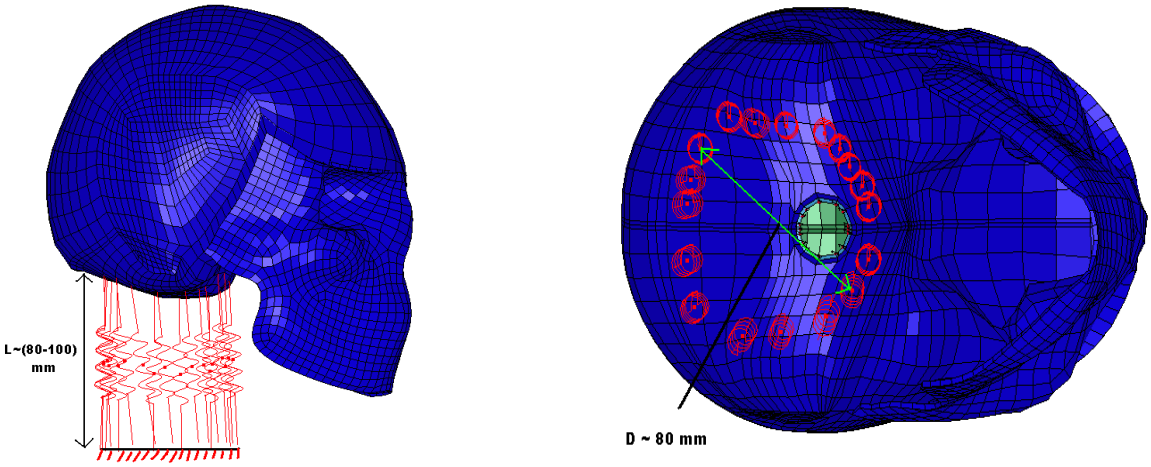

Figure 2-12: The head and neck model for the simulation with the use of springs and dampers (Dirisala et al., 2011).

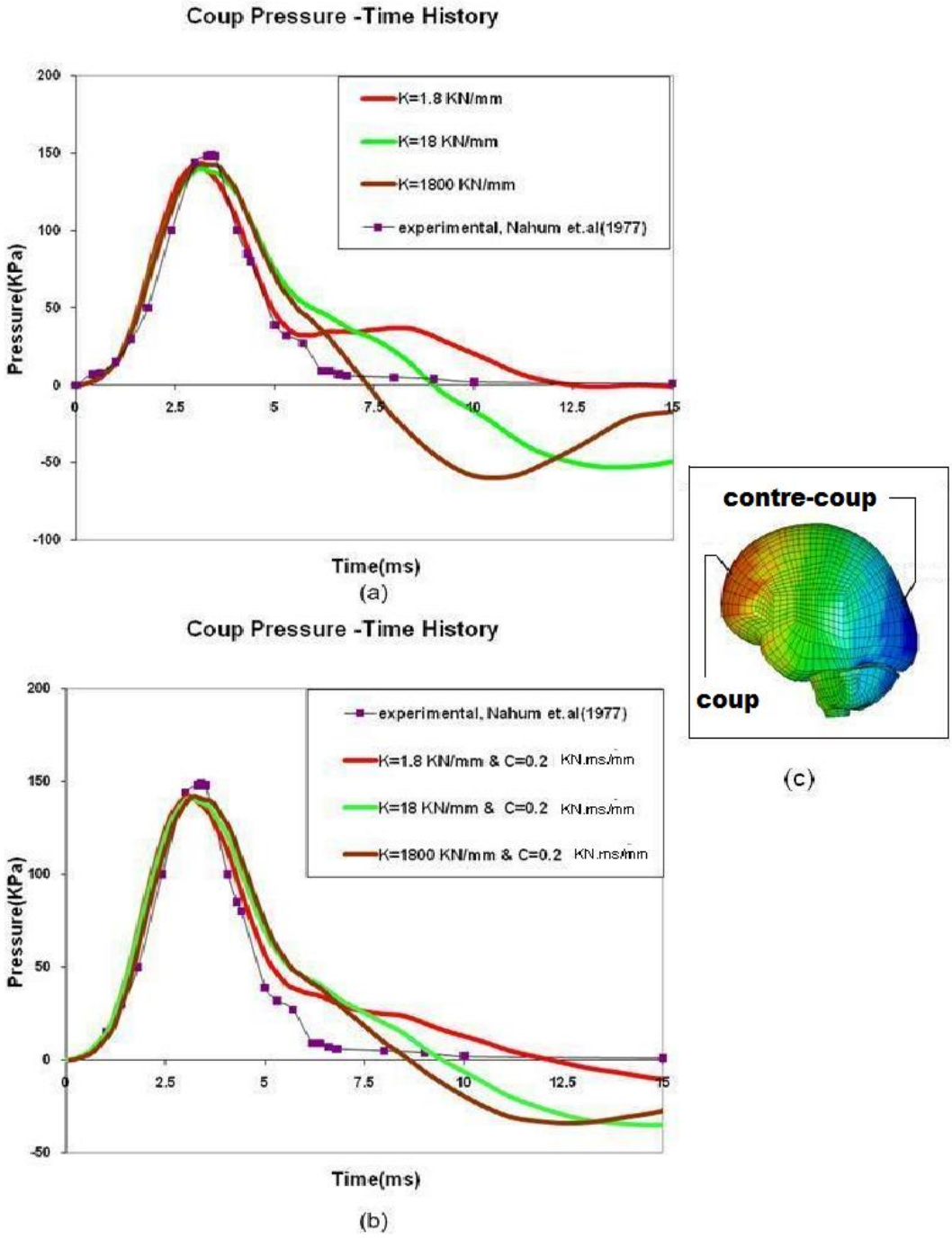

Figure 2-13: Pressure distribution over time on the head model when different damping coefficients are used while a) is using an elastic neck and b) is using a viscoelastic neck. The experimental results are from Nahum et al. in 1977 (Dirisala et al., 2011).

The results of the simulations show that the beginning stages of the movement of the head are not much different from each other, but at the later stages of the movement, the results showed that the intensity of the brain response would be based on the neck damping coefficients. This meant that the intensity of the brain response was going down when the damping coefficient of the neck model was going up after the beginning stage of the movement of the head (Dirisala et al., 2011).

CHAPTER 3. DESIGN AND ELEMENTS OF THE SHOCK TUBE AND EXPERIMENTAL PROCEDURE

This chapter will describe the overall procedures for the experiment presented in this paper, descriptions of the instruments used and the methods used for acquiring the data.

3.1. Experimental Setup

The experimental setup consisted of five major sections: 1) the air compressor; 2) the driver section; 3) the assembling of butterfly valve, pneumatic actuator, and solenoid valve; 4) the testing section; and 5) the data acquisition section. Figure 3-1 is a brief sketch of the setup.

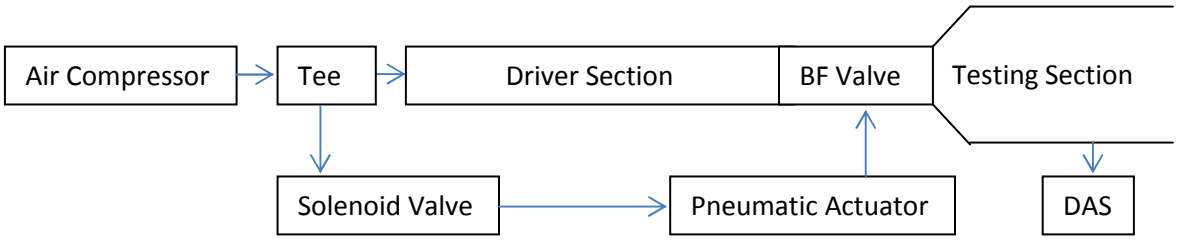

Figure 3-1: An overall look at the experimental setup.

3.1.1. Air Compressor

The air compressor provided compressed air needed at a preferred pressure. The air compressor was able to provide a maximum pressure of 175 psi while it had a volumetric flow of 14.7 cubic feet per minute at the maximum pressure. The air pump had a speed of 1575 revolutions per minute. Attached to the air compressor was a gas tank that has a capacity of 60 gallons.

3.1.2. Driver Section

In this section, compressed air was being transferred from the air compressor. The pipe has an inner diameter of 8” while the thickness of the pipe was 3/8”. One end of the tube was closed by welding a slab made of steel while the other end was closed when the butterfly valve operated by the air compressor. The air in this section supposedly compressed down to 170 psi, which is about 11.568 atm. The steel pipe had minimum yield strength of 250 MPa, meaning that the internal pressure created by running the compressed air into the steel pipe was safe. The driver pipe is shown below as Figure 3-2.

Figure 3-2: The air storage section (driver section) and the two stands holding the shock tube.

The total length of the steel pipe between the closed end and the butterfly valve was 289.5 inches. When adding the weight of the flanges, the total weight of this section was then about 971 pounds. To lift the weight of this pipe of the shock tube, there were two steel stands made and bolted to the flanges, which were welded to the outer surface of the pipe. The frames were made by using two inches by two inches square tubing, with a thickness of a quarter inch, and angles that were welded to the frames so anchor bolts could go through the angles and be bolted to the concrete floor.

3.1.3. Solenoid-Controlled Pneumatic-Actuated Butterfly Valve

As described in Section 3.1, the valve assembling involved the assembling of a butterfly valve, a pneumatic actuator, and a solenoid valve.

The high performance butterfly valve had the standard wafer pattern meaning that there were only two holes that could be used for bolting the valve to the flanges. The butterfly valve and the steel flanges all had the same 300 lbs rating so they could handle a higher pressure and the valve size was 8 inches so it matched the size of the pipe and the flanges. As the operating speed of the butterfly valve was the priority of this experiment, a pneumatic actuator is chosen instead of an electric actuator. An electric actuator would be more convenient, but the fastest electric actuator for this size still needs about 10 seconds to operate. A pneumatic actuator was the choice, therefore, as it could make the butterfly valve open within a second. The selected pneumatic actuator was a spring return type, meaning that when the actuator was filled with air, the butterfly

valve would begin to turn. When the valve was turned 90 degrees and closed, the valve could spring back open by pressing a button.

Although a pneumatic actuator was a good choice and it did what it needed to do, it did have some limitations during operations. The two major limitations were the pressure range and the other is the temperature range. The pressure range was between 40 and 120 psi, meaning that the experiment would be fine when the operating pressure was not higher than 120 psi and not lower than 40 psi when the operating temperature was between -4 and 176 degrees F.

The solenoid valve is an electro-mechanical valve that is mostly used for experiments that involve air or fluids. The main purpose of the valve is to control the air flow, which comes from the air compressor. By using the solenoid valve, the compressed air used to operate the pneumatic actuator and the butterfly valve can be released and the butterfly valve can then spring back to its original position at high speed. The solenoid valve is designed to mount directly to the pneumatic actuator so they can operate together. The solenoid valve has a flow coefficient of 1.4. Similar to the pneumatic actuator, there are some limitations for operating the solenoid valve. The operating temperature is between 20 and 125 degrees F, while the operating pressure is between 5 and 115 psi.

3.1.4. Testing Sections

This section was previously designed to have a removable cross-sectional area chamber pipe larger than the driver pipe. When the chamber pipe was used, the Hybrid III Dummy Head was constrained by four collars so that there would be no movement on the base of the dummy head. The chamber pipe had

a length of 6 feet, an inner diameter of 15 inches and an outer diameter of 16 inches. One end of the chamber pipe was welded to the flow widener, and the other end was open. There was also a hole with a diameter of 8 inches midway through and at the bottom side of the pipe. The purpose of the hole was to allow the dummy head to go through the hole and be placed inside the chamber.

When the testing chamber pipe was not attached to the stand, the movement/reaction of the dummy head could be determined when the dummy head was being hit by the pressure pulse and slides through the rail system.

The testing section had a length of 110 inches, and it had an estimated weight of 600 lbs, including the flanges used to bolt the pipes together. To withstand the weight, another stand with similar design to the stands was made to hold the pressurized air storage pipe is made.

3.1.5. Data Acquisition

A data acquisition system was used to obtain useful data from any sensor so that the data could be transferred to a computer. In this experiment, SCC-68 made by the National Instruments was the input/output connector block used. Connected to the connector block by using wires, it helped connect the circuit board to the power supply, and to the load cell sensor. The other side of the connector block was connected to the circuit and to a computer by using a specific cable and a card device.

To get the acceleration results, two accelerometers were used. Both accelerometers were attached to a wood block, which was mounted to the load cell by using bolts and nuts. The two accelerometers were used to measure the

accelerations of the dummy head in two different directions. One was the direction of the head sliding through the rail, which was assumed to be x-direction. The other accelerometer measured the acceleration of the dummy head in its left/right direction, which assumed to be y-direction.

3.2. Dummy Head/Neck

The dummy head/neck used in the experiment was the Hybrid III 50th Percentile Male Crash Test Dummy Head/Neck, and it was made by Humanetics. The dummy itself is model used popularly in many different types of crash tests and regulated by USA Code of Federal Regulations.

The skull and skull cap of the head model made of cast aluminum, while the removable skin of the head made of vinyl (type of plastic). The neck consisted of rubber and aluminum while there was a center cable inside the neck, so that the model was able to have an accurate reaction due to any sudden change of environment. Figure 3-3 shows the side view of the dummy head/neck.

Figure 3-3: The actual Hybrid III 50th Percentile Male Crash Test Dummy Head/Neck.

3.3. High Speed Camera/Computer/Motion Studio

Some of the experimental results were obtained by using the tracking function from a high speed camera and Motion Studio software, which installed into a computer. When the test was performed, the frames were captured by the high speed camera and then transferred to the computer. The Motion Studio software was able to analyze the work and useful data could then be obtained. The camera was set 140 inches away from the center point of the shock tube opening. To use the tracking function of the high speed camera, a reference point was needed, and was selected to be the center of gravity point of the dummy head as shown in Figure 3-4.

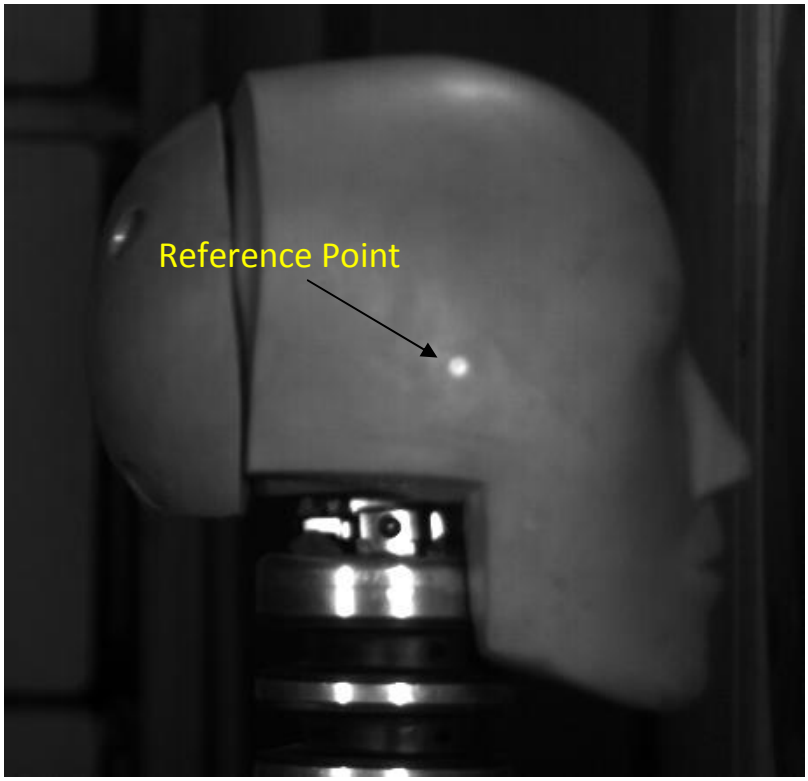

Figure 3-4: The Hybrid III Dummy Head with the reference point from the camera view.

The Motion Studio software was to track the reference point while the dummy head was hit by the blast and sliding through the rails. The test gave the values of displacement, velocity, and acceleration in both the x and y directions.

3.4. Experimental Procedure

With there being many subsections for this experiment, the entire procedure was somewhat complex. Before turning on the air compressor, the hoses needed to be connected to the pipe, and the solenoid valve, and the air compressor needed to be tight. The next step was to assure that the valve of the air tank and one of the valves at the tee (In this case, the solenoid valve) were open. Finally, the air compressor needed to be turned on so it could start pumping air into the solenoid valve through the hose.

The maximum operating pressure was about 115 psi, and air was pumped into the solenoid valve until the air pressure reached a preferred pressure that was less than 115 psi. As the air pressure was increased, the butterfly valve started turning, until it finally was at its closed position.

The next step was to close the opened valve and open the closed valve at the tee so that the air could start getting pumped into the compressed air storage section pipe. The air pressure inside the storage pipe was increased to about 100 psi, and could be checked by looking at the pressure gauge at the end of the pipe. When the pressure got up to 100 psi, the air compressor could be turned off and all the preparations were complete. The test was then ready to proceed.

With everything ready, the test began by pressing the red button on the solenoid valve. Before running the test, the dummy head needed to be secured

correctly and ear plugs were needed as it was anticipated that the blast created by using the shock tube would be extremely loud. By pressing the button, the air controlling the pneumatic actuator and the butterfly valve were released and the butterfly valve returned to its original opened position. By the time the butterfly valve was opened, within less than a second, the compressed air inside the driver pipe flowed through the valve and the air flowed into the chamber pipe. Part of the air hit the dummy head, some air circulated inside the chamber pipe, and the rest exited at the open end of the chamber pipe.

CHAPTER 4. EXPERIMENTAL RESULTS AND DISCUSSIONS

There was a total of 27 tests performed and used for this research. The first parameter to be considered was the bending movement of the dummy head/neck that led to a change of the expected results. When the head/neck bending backward, the change of the velocity was supposed to be slightly increased so that the slope of the velocity curve was a little steeper than when the head/neck was not bent. After the bending of the head/neck, it then bounced back to the original position, which caused the dropping of the velocity or the dropping of the change of the velocity. After the short period of time of bending of the head/neck, the velocity curve starts going back up once again until the friction of the rail is slowed down the movement of the head/neck. Figure 4-1 shows the difference of velocity between different pressure pulses over a period of time, while the reference point of the head/neck is set five inches away from the shock tube opening. The velocity would be most affected when a higher pressure pulse is used for testing. The higher the pressure pulse, the larger the angle of the neck would be bent, plus the curve for lower pressure pulse would be smoother than the curves for higher pressure pulses.

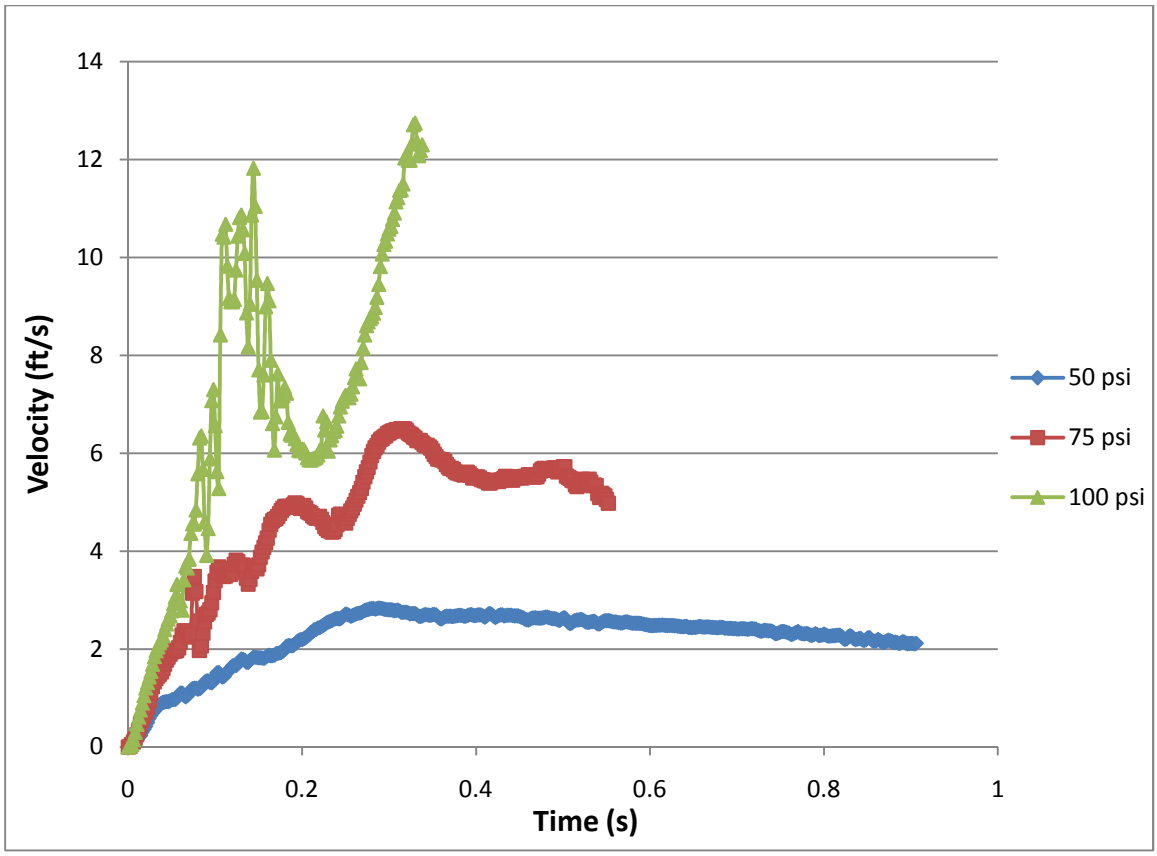

Figure 4-1: The velocity plot with different pressure pulses being used over time.

The second parameter was the rippling of the rubber face. As the rubber face rippled when the blast hit, the results were affected when the tracking function of the high speed camera was used. Such results would not be affected if accelerometers were used. The third parameter was the friction caused between the rail and the sliding plate and how it varied the results. As the rail had a specific friction coefficient, the testing could not be assumed to be in a free space environment. The friction coefficient is calculated to be about 0.03 after the use of a force gauge.

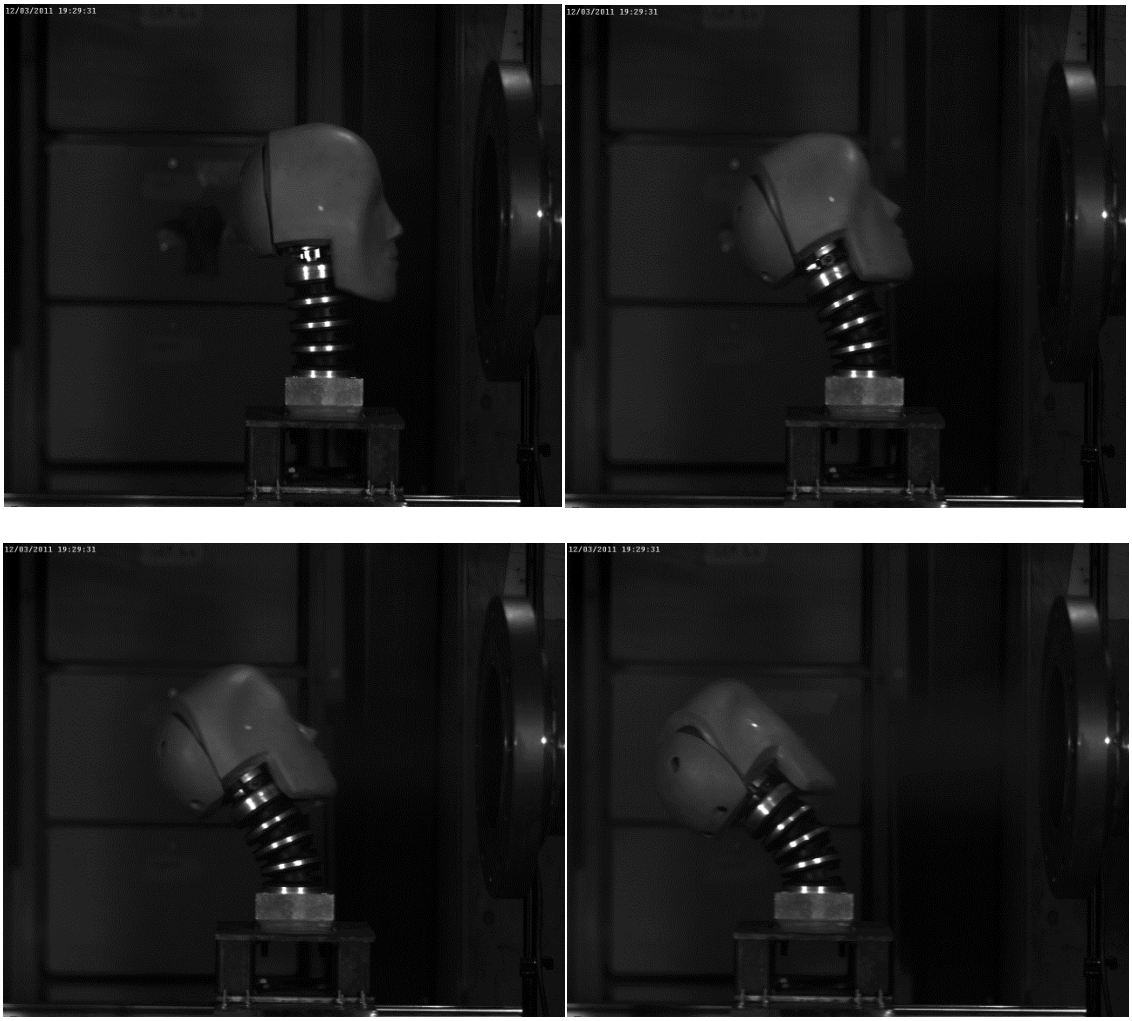

Figure 4-2: Rippling of the rubber face during testing at different time.

4.1. Tracking Results

The following plots (Figure 4-3) show the difference on linear acceleration when different pressure pulses are used. The results are based on the data obtained by using the high speed camera, with a unit of g that represented the gravitational acceleration.

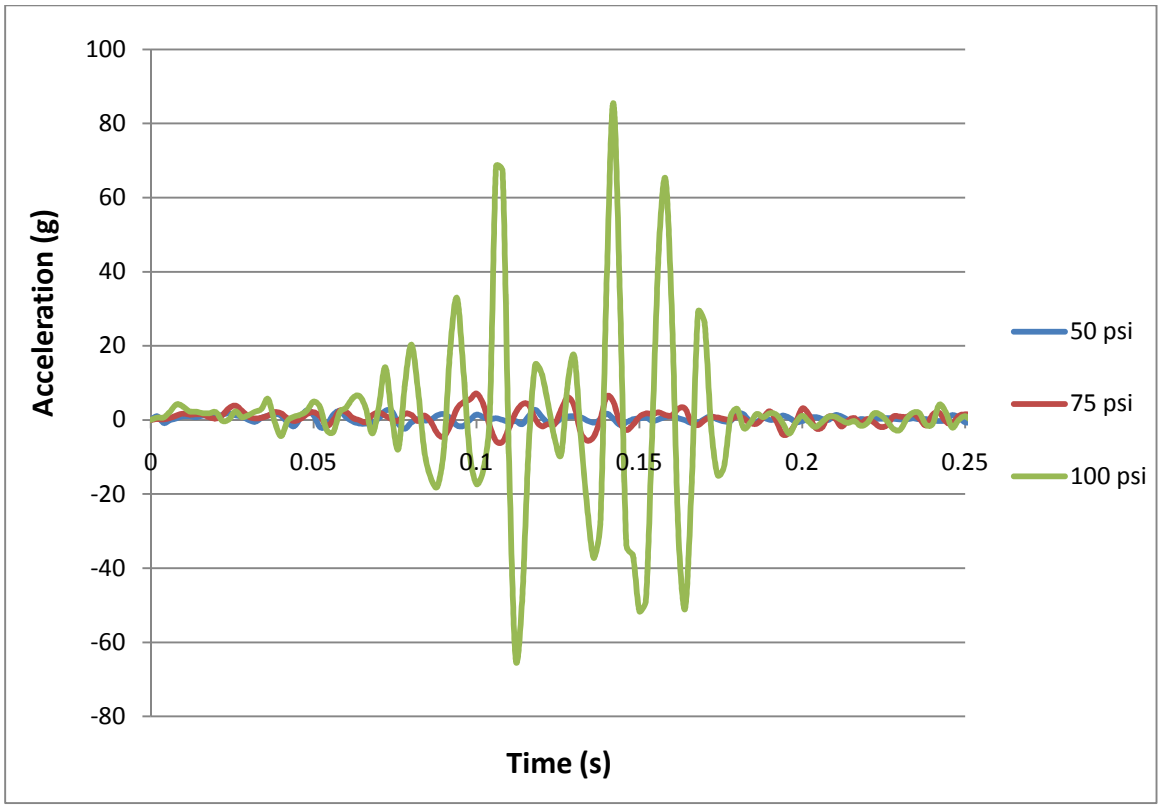

Figure 4-3: Acceleration over time plot with three different pressure pulses when the reference point on the dummy head is 5 inches away from the shock tube opening.

Figure 4-3 shows that the acceleration with a 100 psi pressure pulse had a much higher magnitude than the other two curves, which were based on 50 psi and 75 psi pressure pulses being used for testing. When the acceleration curve for the 100 psi pressure taken away, there was not much change in acceleration between the two cases as shown Figure 4-5.

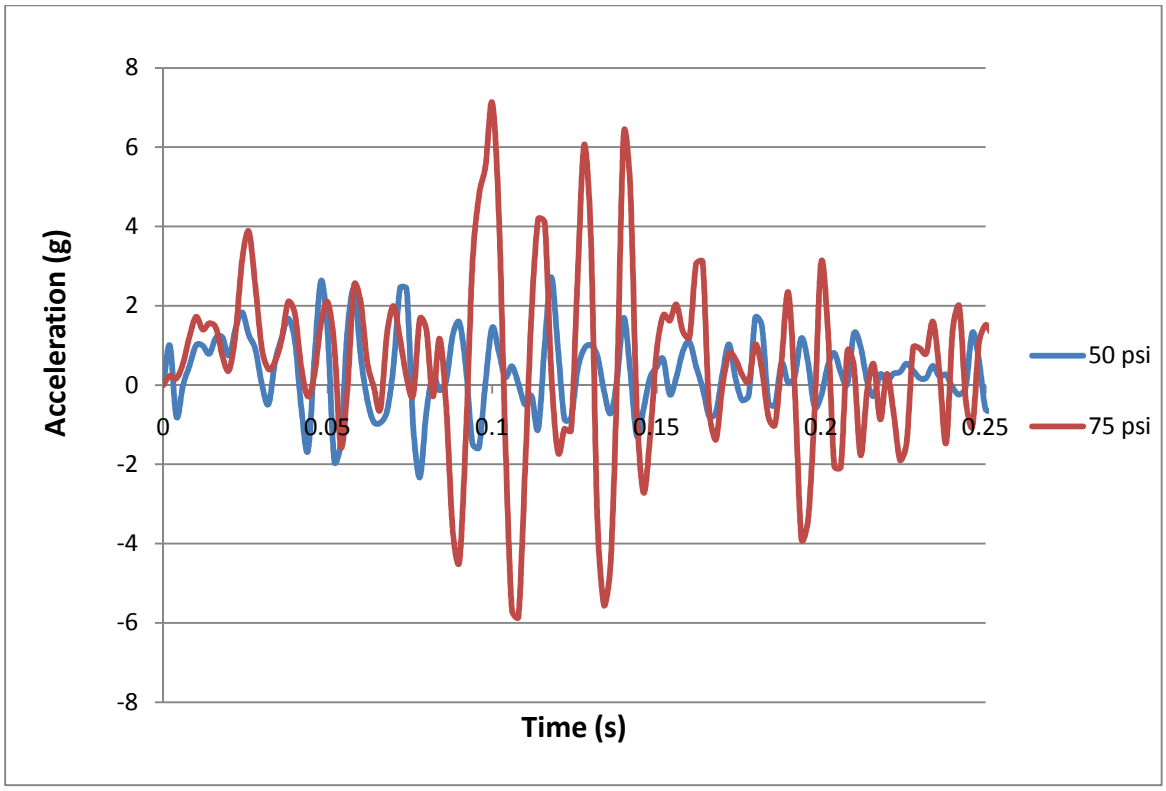

Figure 4-4: Acceleration over time plot with only 50 and 75 psi pressure pulses.

The time plot shows that even without the acceleration curve of the 100 psi pressure pulse, the maximum acceleration based on the 75 psi pressure pulse was about three times larger than the maximum acceleration based on the 50 psi pressure pulse tests.

Other than finding the difference in the velocity and the acceleration based on different pressure pulses, more testing was done as the head/neck's placement varied. Figure 4-5 shows the effect of the placement of the head/neck on the velocity.

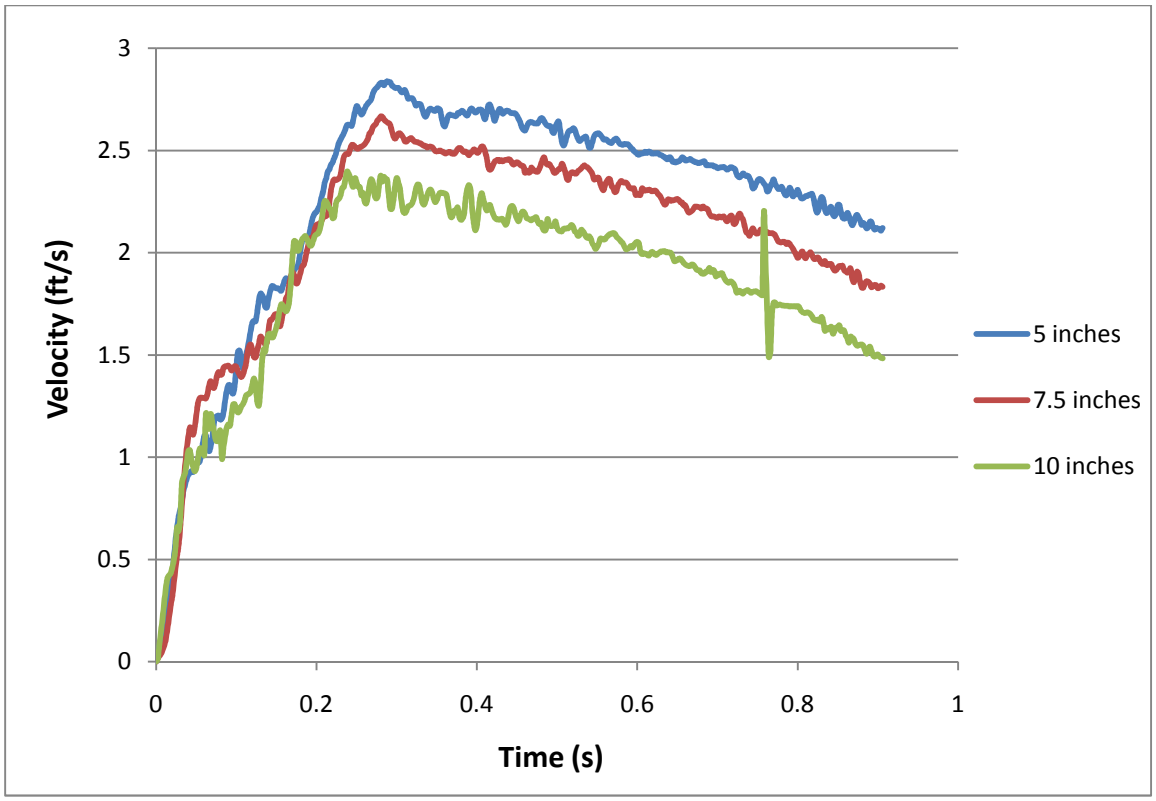

Figure 4-5: Velocity curves over time based on different placements of the head while 50 psi pressure pulse was used.

The plot above shows the difference between three placements of the head/neck away from the shock tube opening, and the results shown in the plot are based on 50 psi pressure blasts. As expected, the closer the head/neck to the shock tube opening, the higher velocity values. In addition, as the shock wave was not strong enough, the effect caused by the bending movement of the head/neck was not as much. Figure 4-6 is the plot for the velocity curves over time when the pressure pulse was set to be 75 psi.

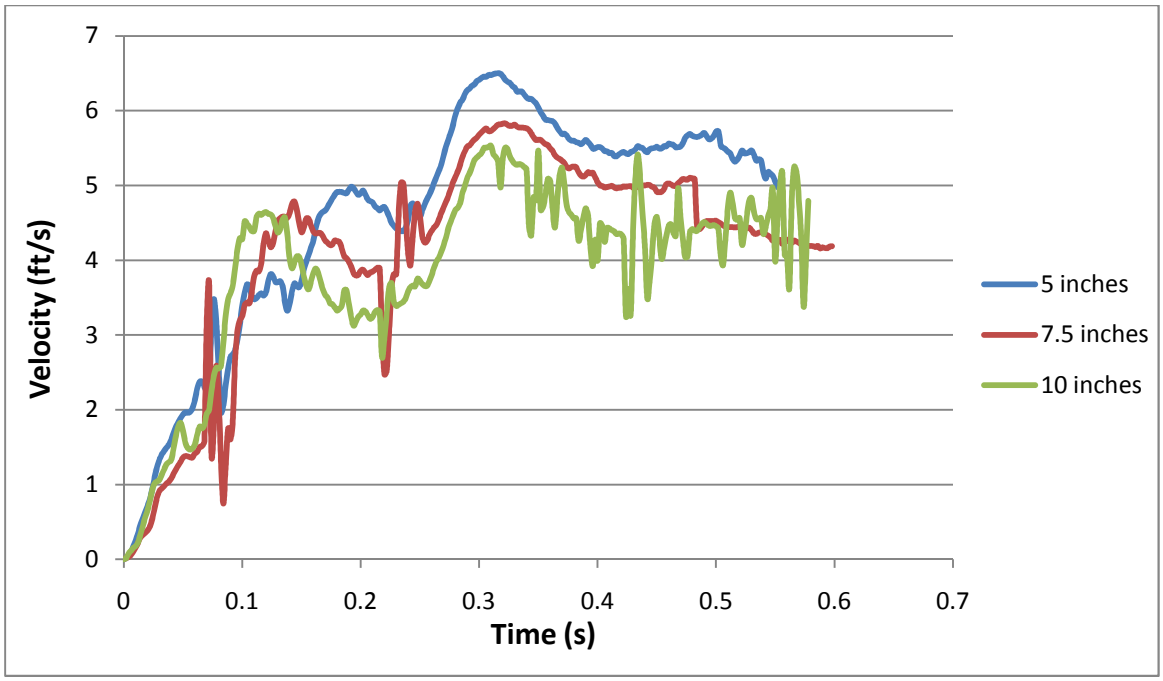

Figure 4-6: Velocity curves based on different placements of the dummy head over time when pressure pulse was set to be 75 psi.

The curves show the instability of the velocity caused by the bending of the head/neck, the rippling of the rubber face, and the friction of the rail that was mentioned earlier. The plot also shows that no matter how the results were affected, the trend was showing that the closer the head/neck to the shock tube opening, the higher the overall velocity.

Figure 4-7 shows the velocity curves over time when the pressure pulse was set to be 100 psi. In this case, the results also show the instability of the velocity caused by the same factors, but that there was no significant difference between the three scenarios. Overall, the two curves representing the head/neck being placed 5 and 7.5 inches away from the shock tube opening were almost the same, while the result for the curve that was set at 10 inches was a little smaller than the other two curves.

Note that the higher the pressure pulse, the shorter the time period. This was due to the speed that the head/neck slid through the rail. The camera did not move horizontally, nor did it keep on tracking on the reference point on the rubber face.

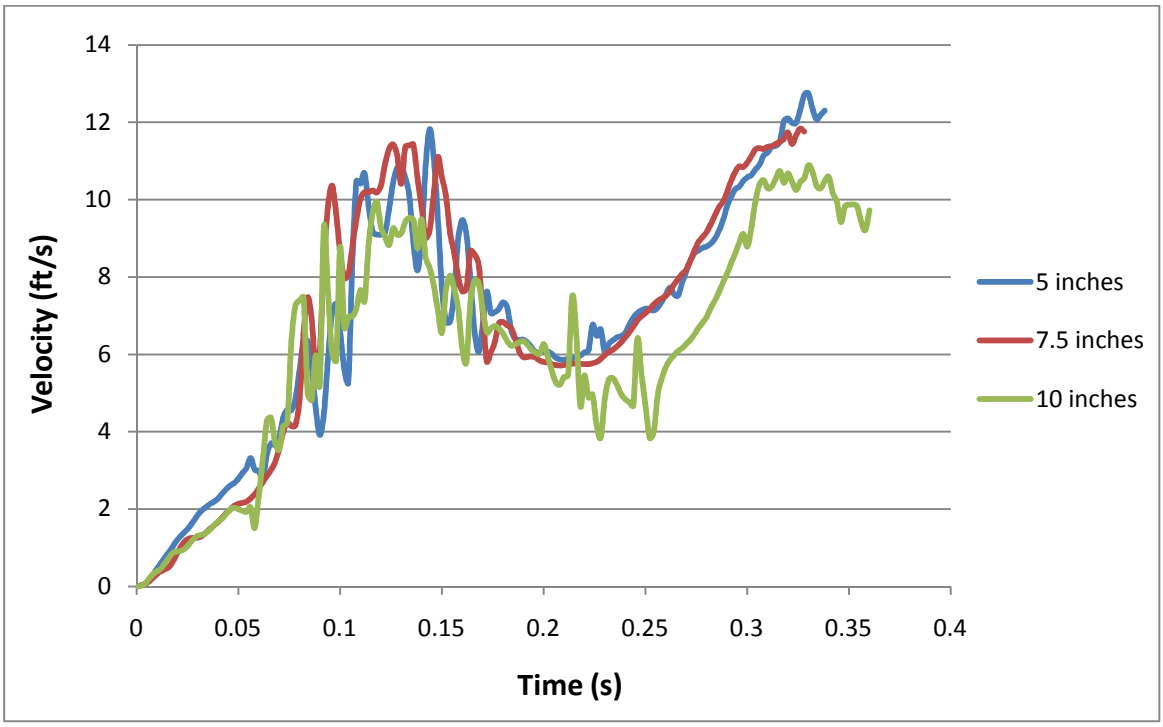

Figure 4-7: Velocity curves based on different placements of the dummy head over time with 100 psi pressure pulse being used.

For the plot in Figure 4-7, the maximum velocity obtained might not be the real maximum velocity, because the data gathered was based on that one reference point. This reference point was supposed to be the center of gravity point, in the frames captured by the high speed camera, while not all the motion of the head/neck was being captured.

If full motion of the head/neck was needed for the analysis, the high speed camera needed to be moved further away, so the motion of the head/neck sliding

through the rail could be taken with a new set of distance calibration. The problem that the camera could not be moved any further as the tripod mounted to the camera was already placed against the wall.

The plots in Figure 4.8 show the acceleration reaction over time with different placements of the head/neck. The results shown are based on 50 psi pressure pulses.

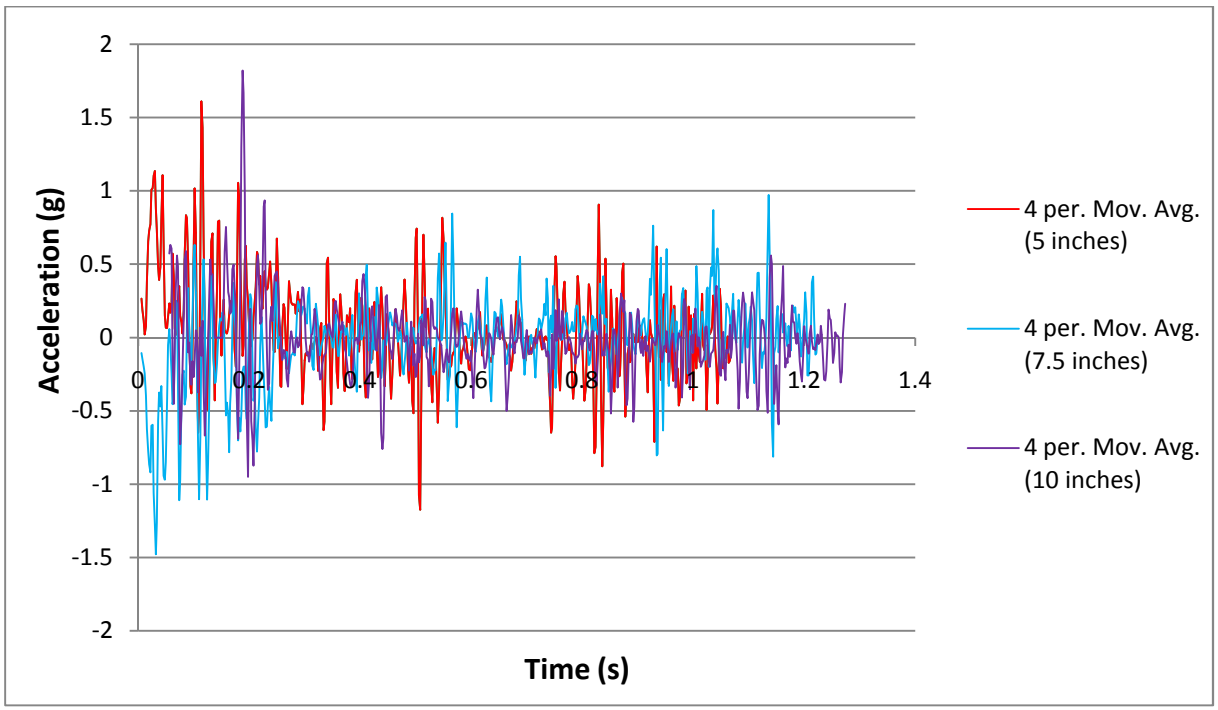

Figure 4-8: Moving average trend lines with 4 periods for acceleration curves over time when 50 psi pressure pulse while the head is placed at 3 different locations (reference point is 5, 7.5, 10 inches away from the shock tube opening).

In the plot above, there are two periods of time that have larger magnitudes in acceleration, which are between 0 and 0.4 second and between 0.8 second and 1.2 second. They seem to have the same trends as the ones

between velocity and time. The closer the head/neck was to the shock tube opening, the higher the maximum acceleration.

As the maximum acceleration should have occurred when the shock blast hit the dummy head/neck, the acceleration at the beginning of the testing should be taken into account for data analyzing, while the second half of the curves could be neglected as the results there were supposed to be minimal. The plot in Figure 4-9 is due to the unwanted vibrations and the second wave of blast hitting the head.

The following plots (Figures 4-9 & 4-10) show the difference between different placements of the head/neck after the second half of the curves got cut off, while 75 psi and 100 psi pressure pulses were used for testing.

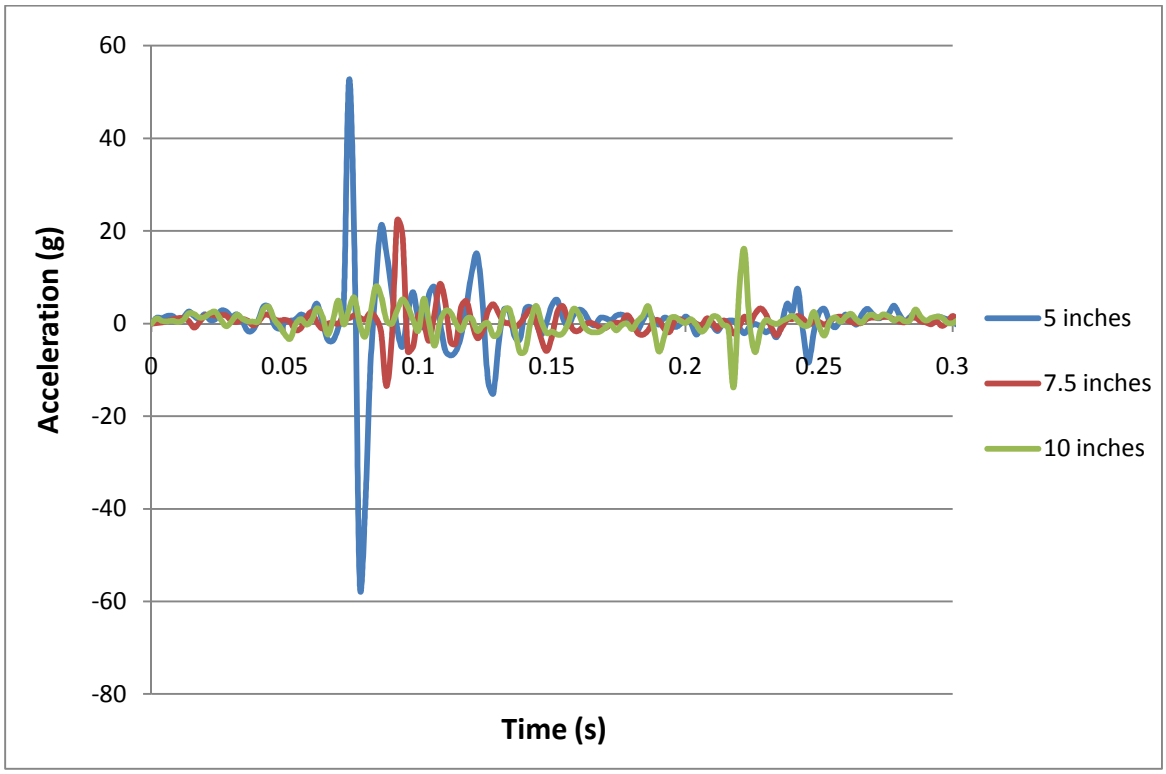

Figure 4-9: Acceleration curves based on different placements of the dummy head with 75 psi pressure pulse being used.

Looked smoother and neater than in Figure 4-8, although the curves were not based on the average of the three tests on each placement, the curves show that the further the head/neck to the shock tube opening, the lower the maximum acceleration.

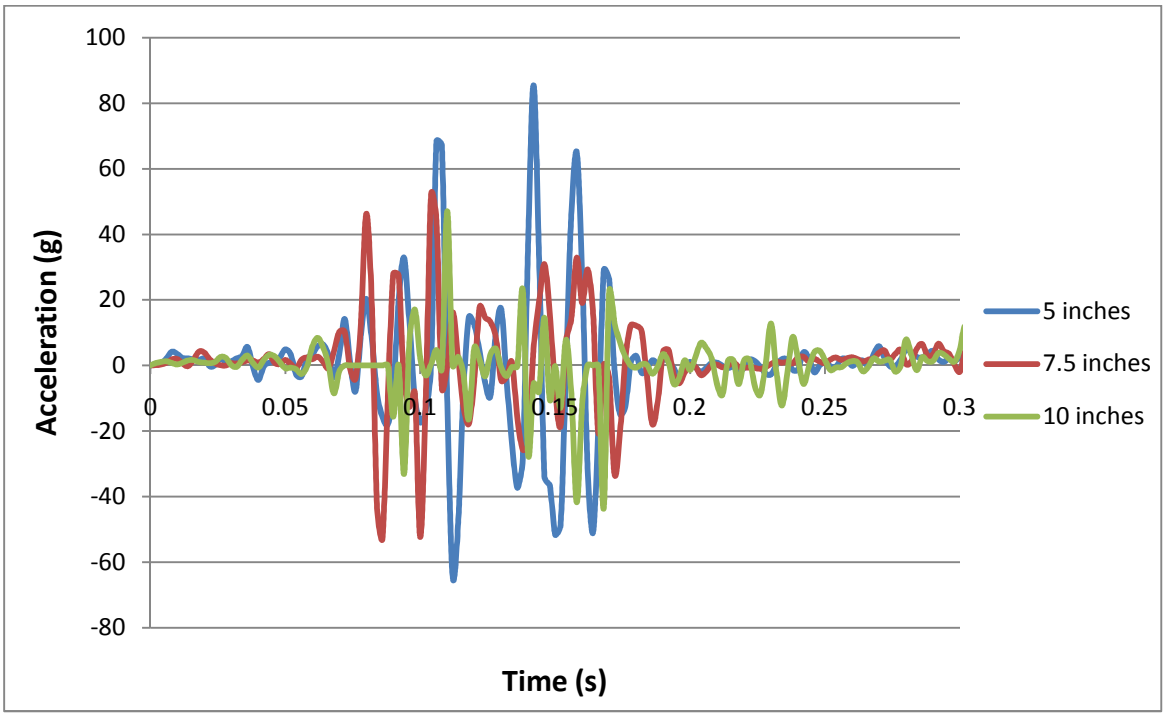

Figure 4-10: Acceleration curves based on different placements of the dummy head when 100 psi pressure pulse is used.

Figure 4-10 shows how the acceleration reacts under a 100 psi pressure pulse. The curves are not as smooth as the ones before that, but the range for the acceleration was increased as the setup pressure pulse was higher.

Using the tracking function from the high speed camera and the Motion Studio software, the maximum velocity and acceleration could be determined. As expected, the velocity started at zero and increased rapidly as the pressure pulse hit the head/neck. Next it started slowing down from the medium and in

this case the air and the friction between the rails and the ball bearings bolted to the sliding plate and the head stand. The maximum velocities for different pressure pulses and distances are listed in Table 4-1.

	5 inches	7.5 inches	10 inches
50 psi	2.839 ft/s	2.667 ft/s	2.397 ft/s
75 psi	6.504 ft/s	5.834 ft/s	5.535 ft/s
100 psi	12.744 ft/s	11.834 ft/s	10.890 ft/s

Table 4-1: Maximum velocities of the dummy head based on three tests on each scenario.

It is shown here that the closer the head/neck to the shock tube opening, the higher the maximum velocity. Although when the pressure pulse was set to be higher, even the placement of the head/neck was placed further, and the maximum velocity was still higher than the one with a lower pressure pulse and shorter distance between the head/neck and the shock tube opening. Table 4-1 shows that the higher the pressure pulse was set for the testing, the greater the difference on the maximum velocity between different placements of the head/neck and the difference between the 5 and 10 inches cases.

Other than finding the maximum velocities of the dummy head, the maximum accelerations on different cases could be found by using Excel. Table 4-2 shows the maximum accelerations obtained by using tracking.

	5 inches	7.5 inches	10 inches
50 psi	3.296 g	2.668 g	2.529 g
75 psi	23.240 g	18.083 g	16.356 g
100 psi	72.820 g	58.852 g	42.324 g

Table 4-2: Maximum accelerations of the dummy head based on three tests on each scenario.

The results are in the unit of g, which is supposed to be gravitational acceleration, while 1 g is the same as $9.80665\frac{m}{s^2}$. Similar to the results of the maximum velocities, the higher the pressure pulse, the higher maximum acceleration, plus the further the head was placed, the lower the maximum acceleration.

Other than finding the relationship between the pressure pulse and the maximum velocity or maximum acceleration, the relationship between the standoff distance and the maximum velocity or maximum acceleration was also found. This is shown in Figure 4-11 using the data from Table 4-1 and Table 4-2.

Figure 4-11 shows that the maximum velocity in all cases dropped when the standoff distance increased as mentioned earlier. When the pressure pulse was increased proportionally, the maximum velocity seemed to increase exponentially. Figure 4-11 also shows that the higher the pressure pulse, the drop of the maximum velocity was faster when the standoff distance was further. A similar situation happened to the relationship between the maximum acceleration and the standoff distance, which is shown in Figure 4-12.

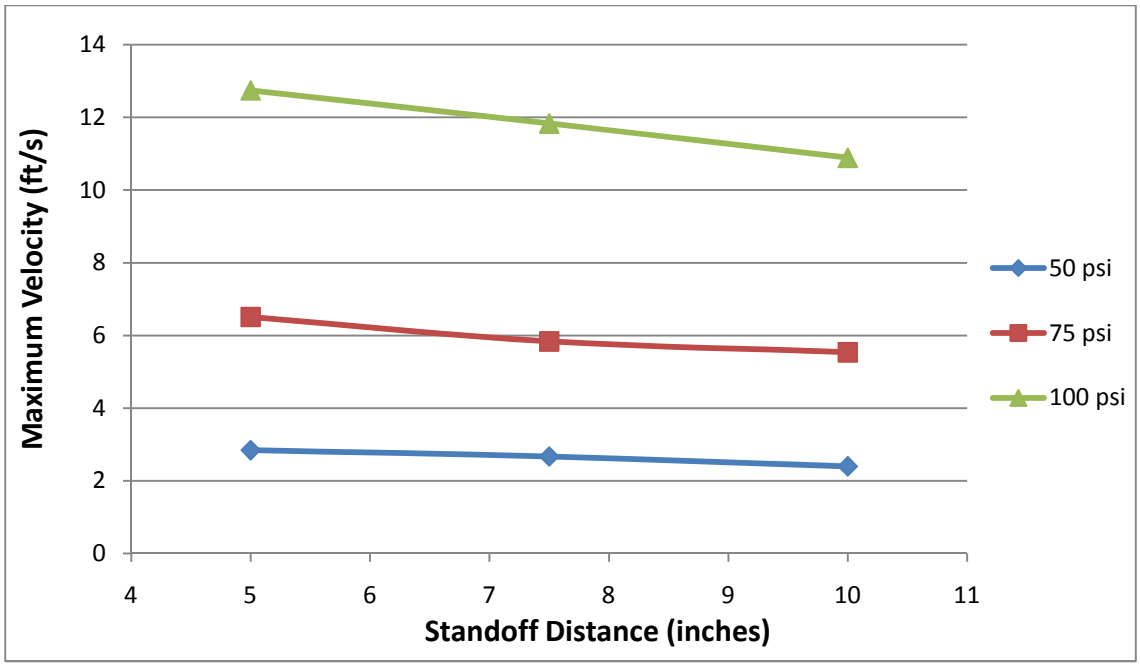

Figure 4-11: Maximum velocity of the dummy head based on different standoff distance (placement).

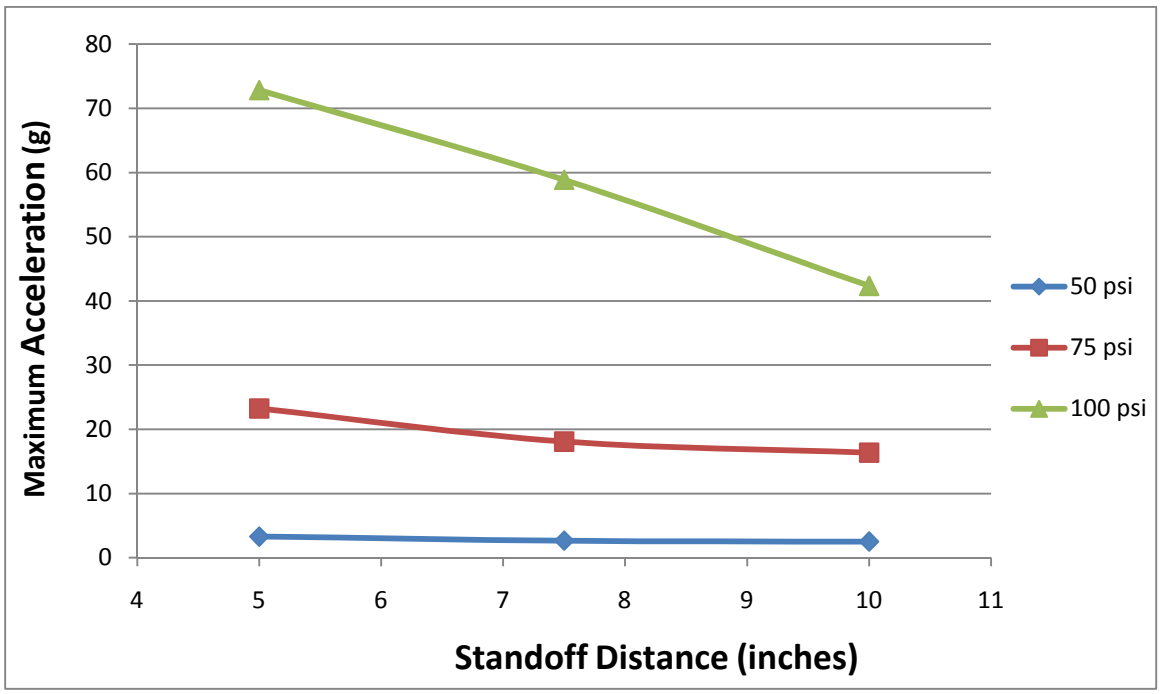

Figure 4-12: Maximum acceleration of the dummy head based on different standoff distance.

4.2. Accelerometers Results

To get the results from using the accelerometers, an additional person was needed for assistance. One person operated the butterfly valve and the Motion Studio software on a computer while the other person communicated and cooperated so he/she would be able to receive data from the accelerometers by using LabVIEW on another computer. The following plot in Figure 4-13 is the result obtained from one of 27 experiments performed.

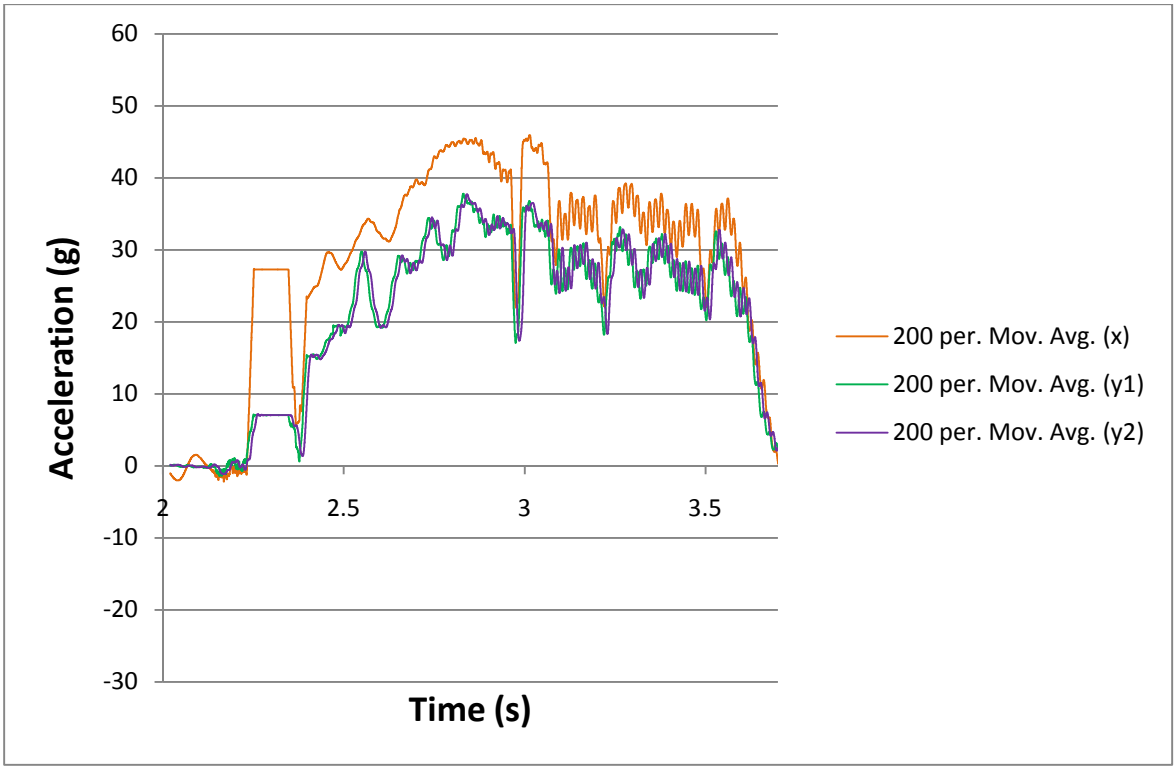

Figure 4-13: Moving average trend lines with 200 periods for accelerations curves with 50 psi pressure pulse is used when the reference point on the dummy head is 5 inches away from the shock tube opening.

Figure 4-13 shows that when the blast hit the dummy head, there was a jump in acceleration, in both x and y directions. The accelerations remained

constant for about 0.2 seconds then began to increase again. The curves finally went back down to about 0 g within time duration of 1.5 seconds. The curves also showed a lot of ups and downs (instability) especially after reaching the maximum accelerations. That was due to the vibrations/movements of the dummy head, or the friction between the bearings and the rails. The plot in Figure 4-14 shows that the acceleration in the x-direction was usually higher than the one in the y-direction, as the dummy head was hit in the x-direction. Note that y1 is the acceleration curve representing an unfiltered result while y2 is the filtered result for the acceleration in the y-direction.

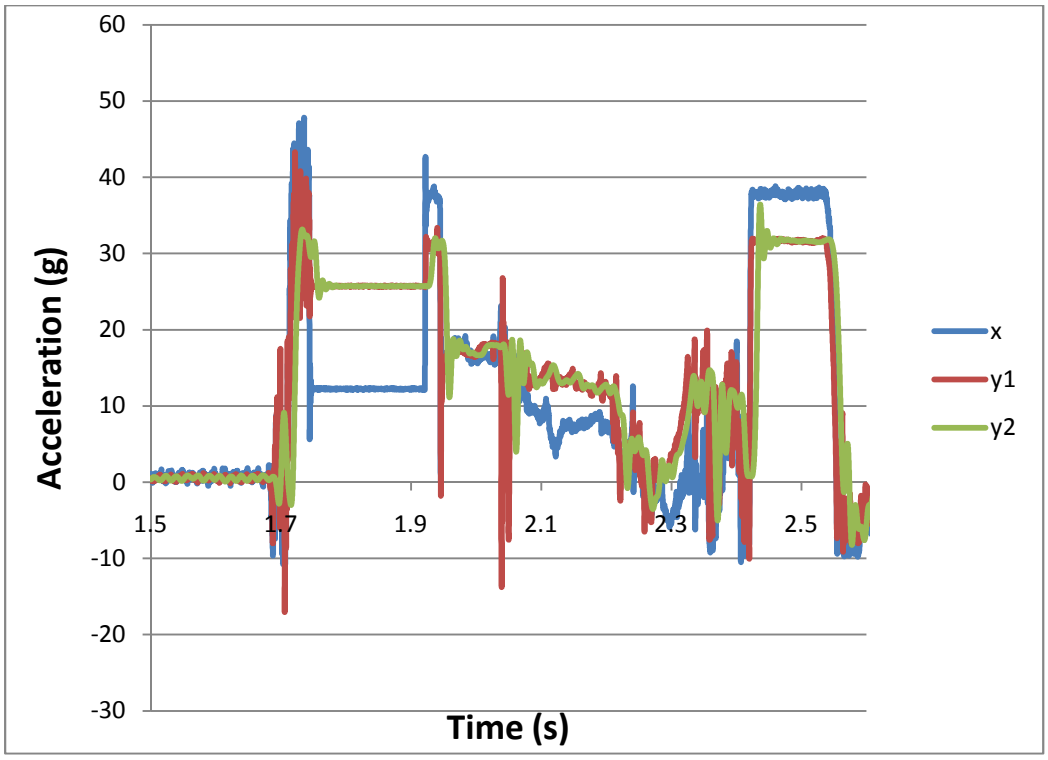

Figure 4-14: Acceleration curves with 50 psi pressure pulse used while the dummy head was set 10 inches away from the shock tube opening.

Figure 4-14 shows the acceleration curves a bit different than the one shown earlier. Similar to the previous plot (Figure 4-13), the acceleration curves on this plot also jumped at the beginning of the test and a constant acceleration phase. Once again the curve started dropping down to about 0 g 0.6 seconds after the release of the compressed air. As mentioned earlier, there was a total of 27 performances conducted for this paper and after receiving all of the data by using accelerometers and some modifications on the data, the maximum accelerations in x-direction and y-direction were found, and they are all listed in Table 4-3 and 4-4 with the results in the unit of g.

	5 inches	7.5 inches	10 inches
50 psi	48.39	32.06	38.28
75 psi	50.89	25.72	19.07
100 psi	59.14	32.34	37.34

Table 4-3: Average maximum acceleration of the dummy head in x-direction.

	5 inches	7.5 inches	10 inches
50 psi	58.46	21.67	30.44
75 psi	48.22	17.26	14.49
100 psi	145.88	48.69	21.42

Table 4-4: Average maximum acceleration of the dummy head in y-direction (filtered).

The tables show a trend that when the placement of the dummy head was set to be the same, the testing pressure pulse and the acceleration increased. When the testing pressure pulse was set to be the same, the further the dummy

head was placed away from the shock tube opening and the lower the acceleration. There were some exceptions in some cases, which were due to some errors in the setup or the instability/accuracy of the devices.

After getting all the maximum values of maximum acceleration, they were used to plot the maximum acceleration based on different standoff distances. Figures 4-15 and 4-16 show the relationship between standoff distance and maximum acceleration in both x-direction and y-direction by using accelerometers.

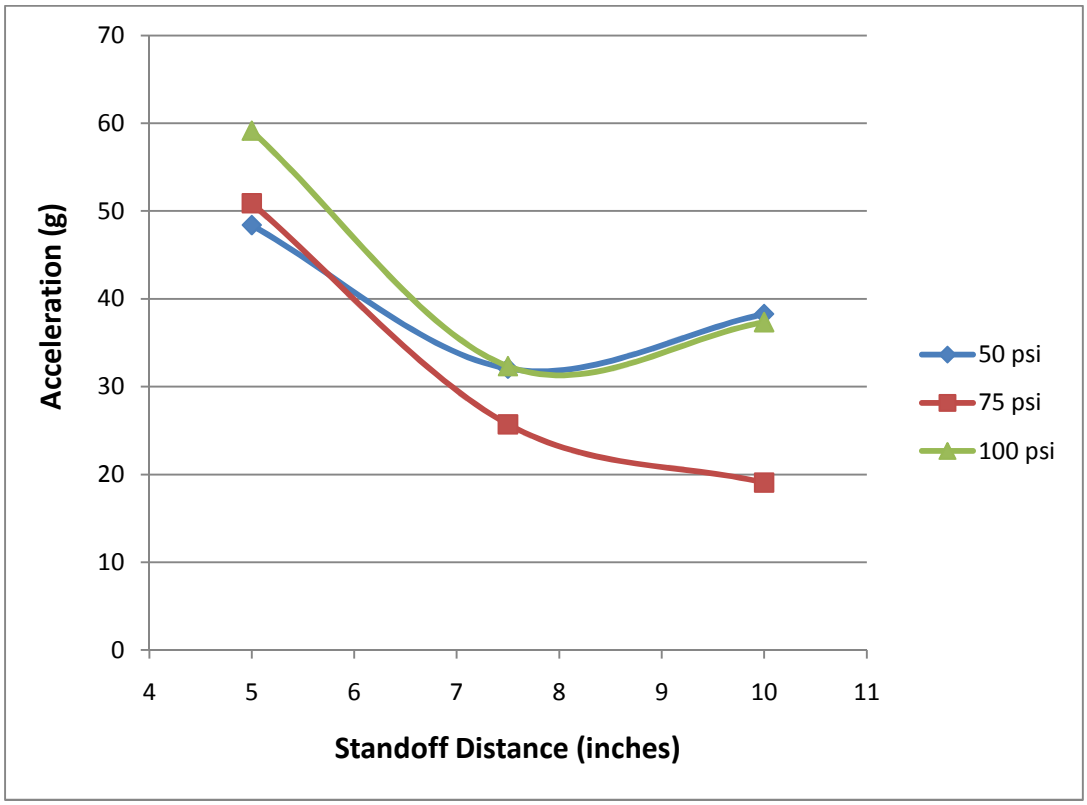

Figure 4-15: Maximum acceleration of the dummy head based on standoff distance in x-direction.

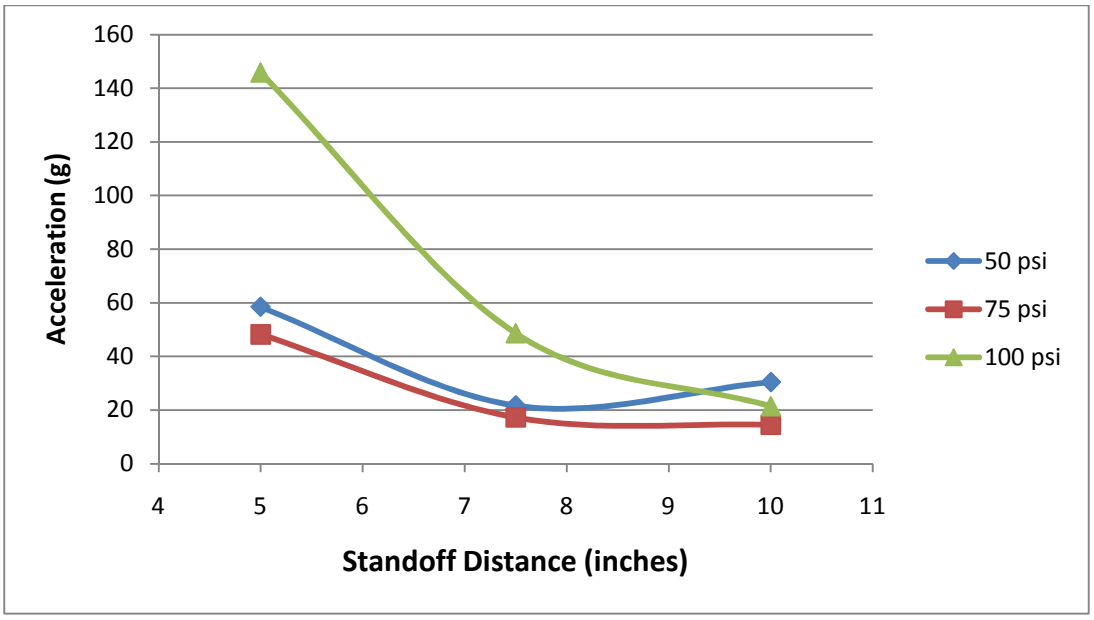

Figure 4-16: Maximum acceleration of the dummy head based on standoff distance in y-direction.

The plot from Figure 4-15 shows that the three curves do not have much difference with the exception of the two curves representing the 50 and 100 psi cases. Those two curves dropped down first, and then went back up a little, which was different than what was expected and what was found by using the tracking of the Motion Studio software and FEA simulation.

Figure 4-16 shows the acceleration results of maximum acceleration in y-direction. The curves show the dropping of maximum acceleration when the standoff distance increased, but there is an error in that the 75 psi curve was always lower than the 50 psi curve. This may be due to the inaccuracy of the device, the reading of the LabVIEW software or some other unknown factors.

CHAPTER 5. FINITE ELEMENT ANALYSIS OF THE SHOCK TUBE FLOW

This chapter is to describe the procedures for the FEA including the descriptions, assumptions, and boundary conditions of the model that is being used. Then results from this specific analysis are also shown.

5.1. LS-DYNA FE Software

LS-DYNA is used to simulate the motion/reaction of the Hybrid III dummy head under shock wave of blast. LS-DYNA is mostly used for transient dynamic FEA on more complex or real life problems, especially in the automobile and the aerospace industries. This software helps in finding a wide variety of results depending on what is wanted, such as the animation of the pressure, velocity distributions of the result, pressure, velocity, acceleration, displacement, or energy plots over a period of time on either a single node or a single element.

5.1.1. Preliminary Shock Tube Model

The model is made by using modeling software HyperMesh of the Atlair Engineering Company. In HyperMesh, the geometries and meshing of the model are done before being exported to LS-PrePost, where conditions would be done at. Figure 5-1 shows what the model looks like.

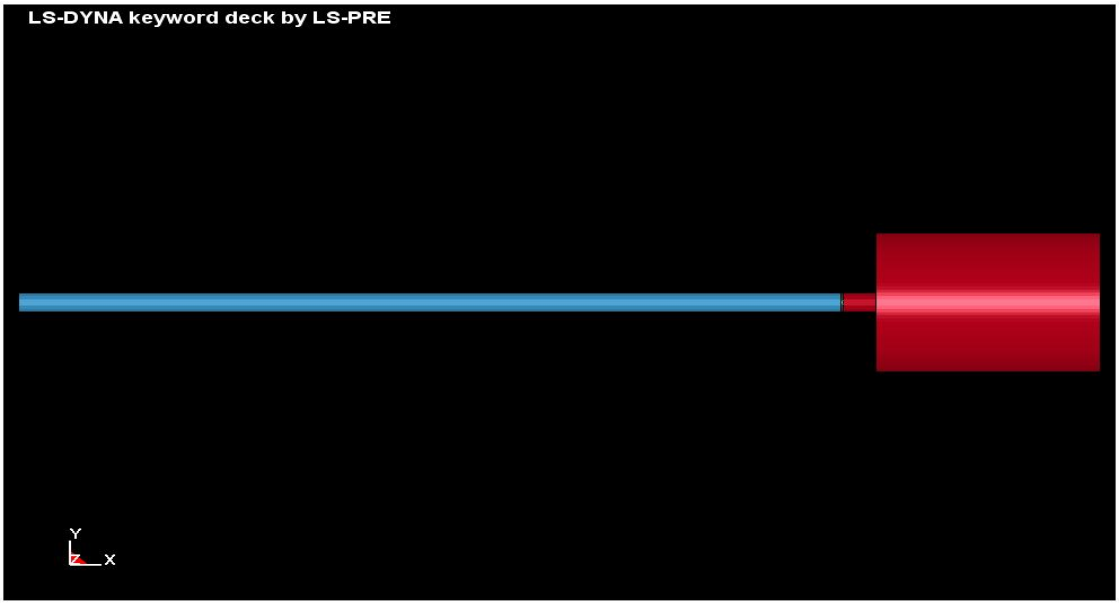

Figure 5-1: Preliminary shock tube model in LS-DYNA.

The model has a total of four parts, which include the air inside the driver section pipe, which has a color of light blue; the air with ambient condition, which has a red color; the butterfly valve, which has a green color, and the head model which is a yellow color. The center point of the head was set at 5, 7.5, and 10 inches away from the shock tube opening.

5.1.2. Condition Setups

There were a few conditions applied to the model. First of all, different energies were applied to both air parts of the model, representing the 100 psi and 14.7 psi pressures for the two air domains. A rigid body assumption was then applied to the valve while the valve was constrained in all directions except for the y-direction, so that the valve would turn along the y-axis, as shown as Figure 5-2. The 'Lagrange In Solid' constrain was selected for the head model as the head was in the air domain. Finally, all the outer surfaces were

constrained as it was assumed that they were in the inner surfaces of the shock tube, meaning that there would be no placement, velocity, nor acceleration changes.

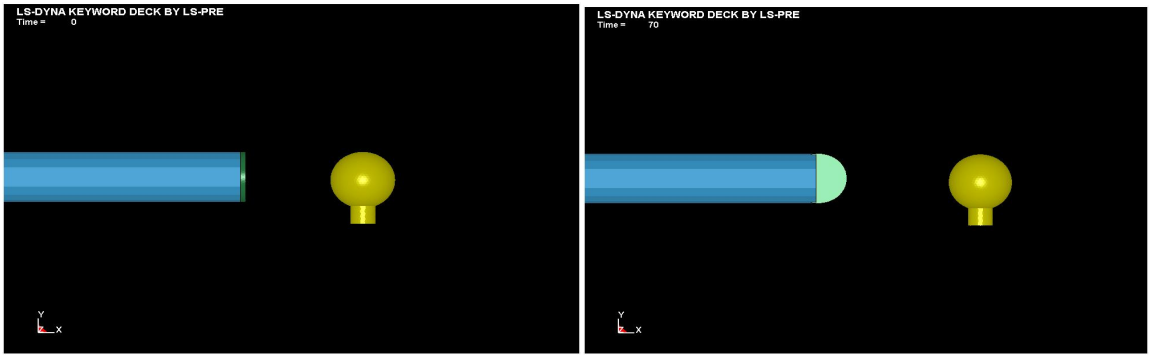

Figure 5-2: a) Initial stage of the model, b) valve is turned 90 degrees.

5.1.3. Numerical Results on the Preliminary Model

After the simulation was complete, the results from the simulation could be shown. Figure 5-3 shows the velocity curves for the results obtained by the simulations.

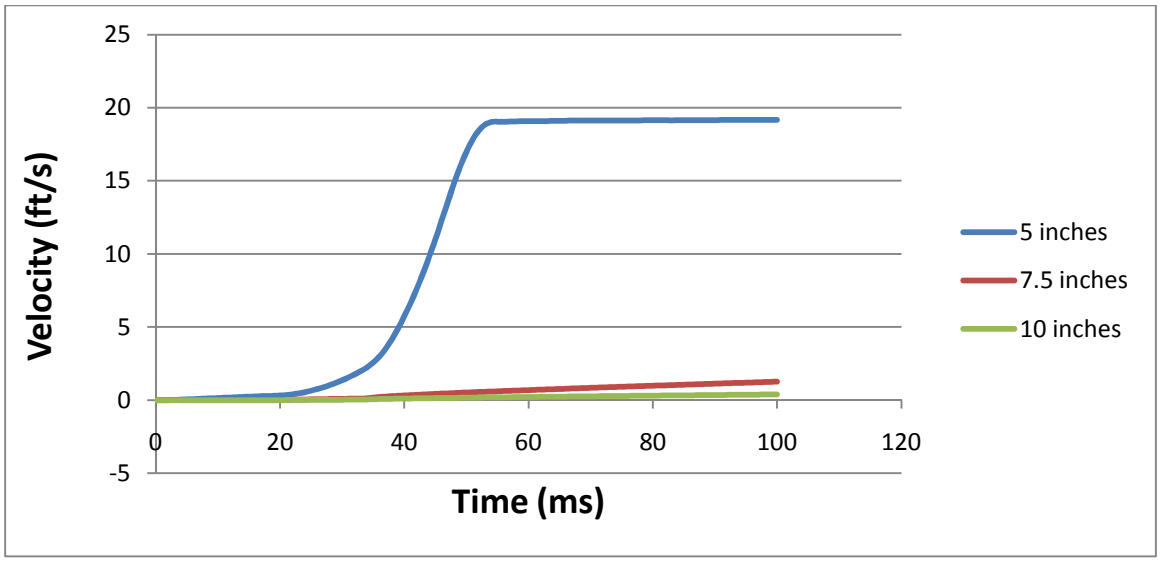

Figure 5-3: Flow velocity with 100 psi pressure pulse.

The plot in Figure 5-3 shows that when the head model was placed 5 inches away from the shock tube opening, the velocity of the head model began to increase at roughly 20 ms after the release of the compressed air. The maximum velocity of the head eventually increased to 19.2 ft/s. The other two curves, representing the cases when the head model was placed 7.5 and 10 inches away from the shock tube opening, were relatively small compared to the 5 inch curve. Although the plot shows that when the head model was placed closer to the shock tube opening, the higher the maximum velocity that it would get.

Figure 5-4 is a plot showing the acceleration curves representing three different areas on the surface of the head model when it was placed 5 inches away from the shock tube opening and the three areas included the front, side, and back of the head model.

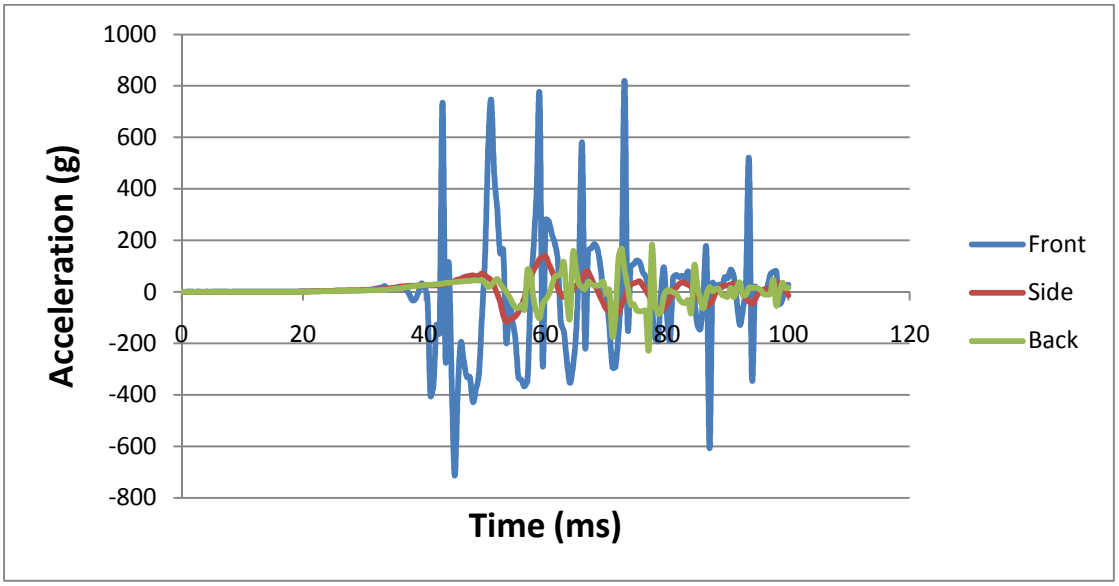

Figure 5-4: Acceleration of the head model when it was placed 5 inches away from the shock tube opening while 100 psi pressure pulse was used.

The plot shows that the frontal area of the head model had the highest magnitude of acceleration (higher than the side and back of the head), while the maximum acceleration on the frontal area topped at 818 g. The maximum values are listed in Table 5-1.

	Front	Side	Back
5 inches	818.08 g	137.71 g	180.56 g
7.5 inches	1.80 g	2.43 g	1.61 g
10 inches	5.78 g	1.44 g	0.89 g

Table 5-1: Maximum accelerations on different spots of the head model.

As shown, the values obtained from the 5 inches case were much larger than those from the 7.5 and 10 inches cases. Such big differences could be due to many factors, such as the energy loss due to the distance between the center point of the head model and the shock tube opening, and the use of the valve model while it took about 0.5 second to finish the 90 degree turn. To verify the use of the valve, a research with experimental results by Varas et al was used.

5.1.4. Validation of existing model using FEM

In a research paper by Varas et al. published in 2011, a square tubing shock tube (Figure 5-5) was used.

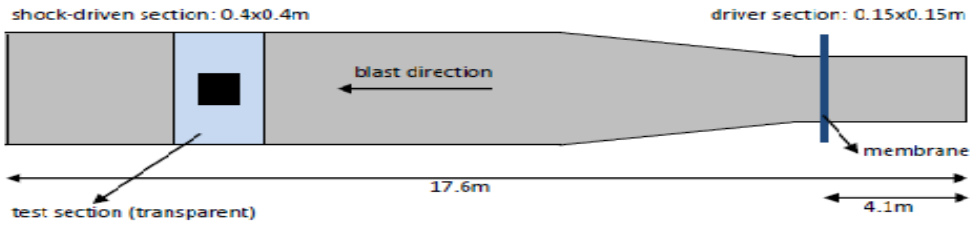

Figure 5-5: Shock Tube by J. M. Varas et al.

The two main differences between Varas' shock tube and the shock tube used for this research were: 1) Varas' shock tube had a square type cross-sectional area instead of a circular type of cross-sectional area, and 2) instead of a butterfly valve operating with a pneumatic actuator, a membrane was being used.

5.1.5. Validation Results

Varas' shock tube had a peak operating pressure of 70 kPa, which was used for the FEA simulation. Figure 5-6 shows the results from Varas' experiment and the numerical results obtained from LS-DYNA.

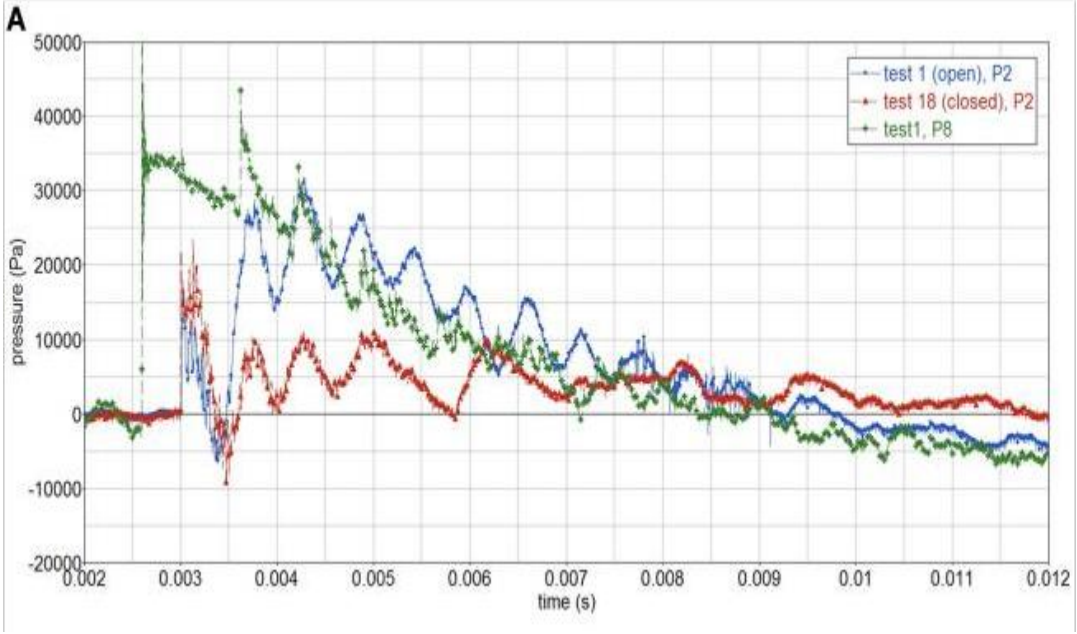

Figure 5-6: Experimental results from Varas' shock tube (2011).

As shown, most of the curves first had a jump on pressure. The pressure then decreased to about zero shortly after the jump, and the jump reached a

maximum pressure of about 34000 Pa. The plot in Figure 5-7 shows that the positive phase of pressure had a duration time of about 7 ms.

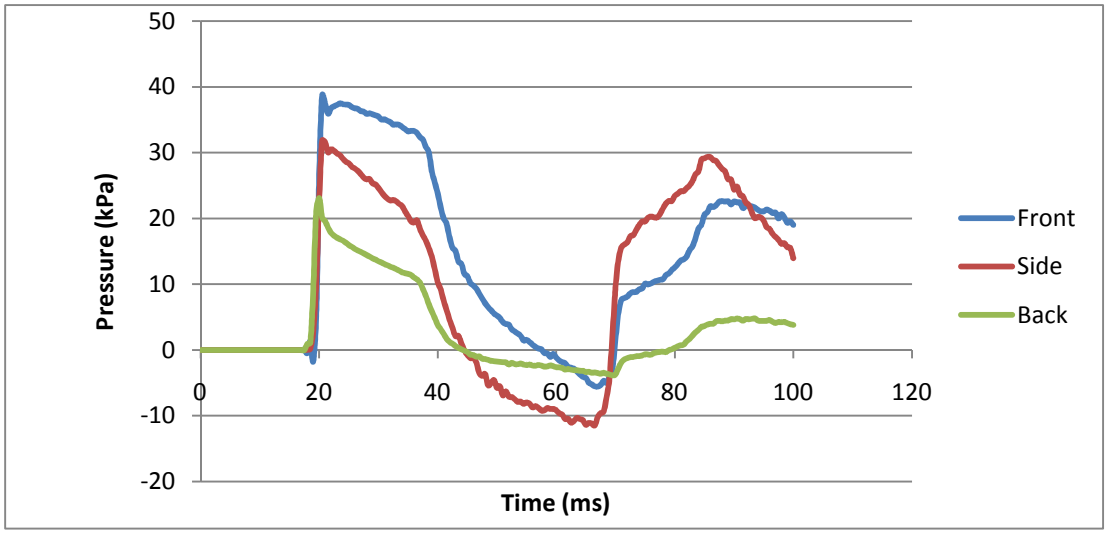

Figure 5-7: Pressure plot based on different areas of the head model.

As shown in Figure 5-7, all of the pressure curves jumped up at about 20 ms, and had a positive phase duration of between 20 and 40 ms. For the curve of frontal area of the head model, the pressure jumped up and topped at about 38 kPa. The pressure on the side area of the head model topped at about 32 kPa. Both were very close to the experimental results obtained by Varas. The main difference was the positive phase time duration. Such a difference would be due to many factors, such as the accuracy of the FE model, the geometry of the whole shock tube, and the model (synbone and gelatin were used for the experimental work and steel was used for the FE model) of the ball.

5.1.6. Modified Model for the Blast Shock Tube

The new model was similar to the previous one used, but the valve was removed. The previous model involved the placement change (5, 7.5, and 10 inches) with one pressure (100 psi), and the new model involved one placement (5 inches) with different pressure pulse sets (50, 75, and 100 psi). Figure 5-8 shows the meshed model with only three separate parts for the simulation.

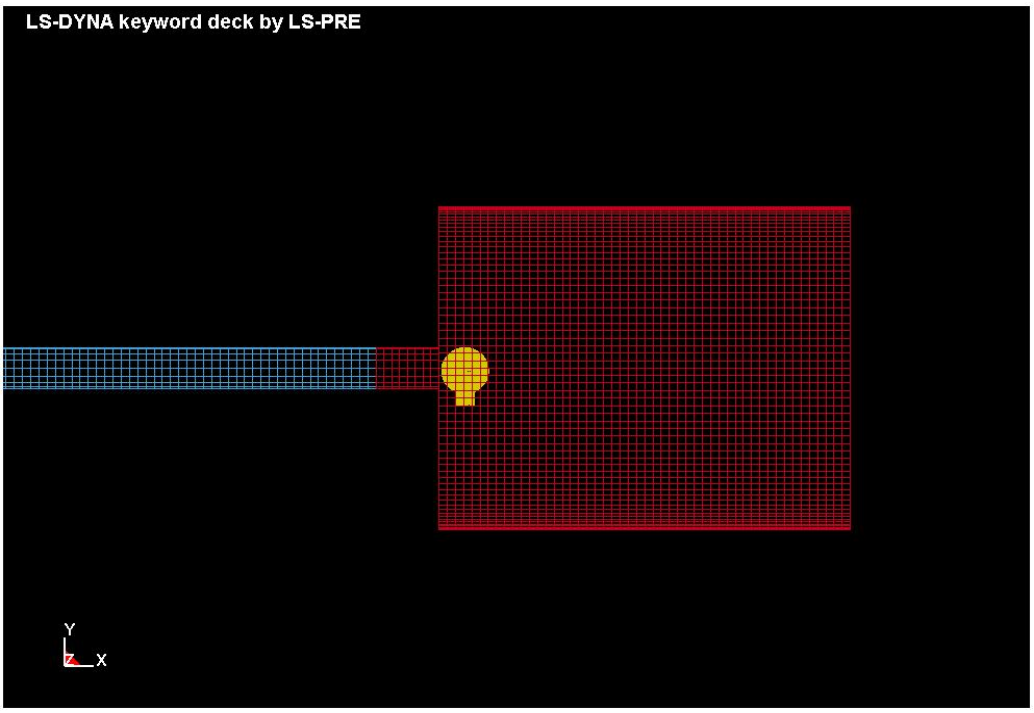

Figure 5-8: Modified shock tube model for simulation.

5.1.7. Results on the New Model

After some changes on boundary conditions, the problem could be solved. Figure 5-9 is the velocity plot for this new shock tube model.

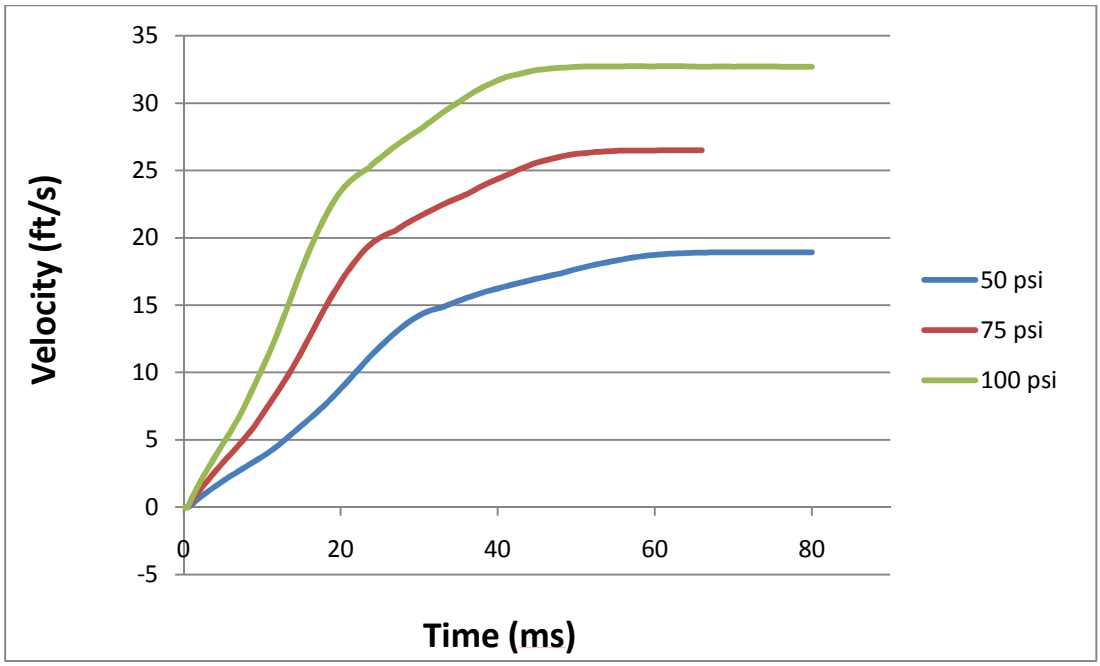

Figure 5-9: Velocity distribution of the head model based on different pressure pulses (50, 75, and 100 psi) when the middle point of the head was 5 inches away from the shock tube opening.

As expected, the 100 psi curve had the highest values among all three cases, then 75 psi had the next highest, and finally the 50 psi curve had the lowest values. This indicates that the higher the pressure pulse, the greater the movement of the head model, or any test object used for the blast. The maximum velocities are listed in Table 5-2.

	Maximum Velocity
50 psi	18.92 ft/s
75 psi	26.51 ft/s
100 psi	32.74 ft/s

Table 5-2: Maximum velocities from the modified shock tube model and head.

Other than the velocity plot, the acceleration plot could also be found by using the software, and Figure 5-10 is an acceleration plot for a specific case.

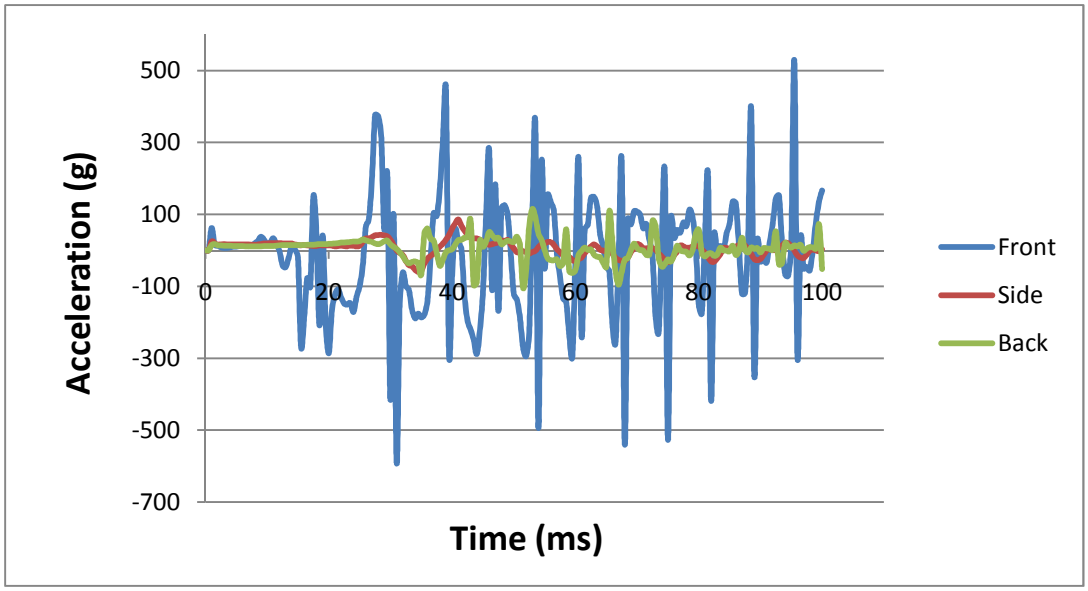

Figure 5-10: Acceleration plot with 50 psi pressure pulse with 5 inches head placement.

The results were similar to the results from when the valve was involved as the frontal area of the head model had the highest magnitude of acceleration rather than the side and back of the head model. The maximum accelerations for the three different cases are listed in Table 5-3.

	Front	Side	Back
50 psi	525.59 g	86.16 g	114.53 g
75 psi	1181.13 g	115.11 g	196.43 g
100 psi	2541.28 g	137.78 g	234.37 g

Table 5-3: Maximum velocities due to different pressure pulses on various spots of the head model.

The acceleration on the frontal area of the head model had a significant increase from the case of 50 psi to the case of 100 psi, which had a difference of about 2000 g. The differences on the side and back of the head model were relatively small compared to the result for the frontal area case, meaning that the acceleration on the frontal area of the head was affected the most when the pressure pulse was changed. Such affect is plotted in Figure 5-11.

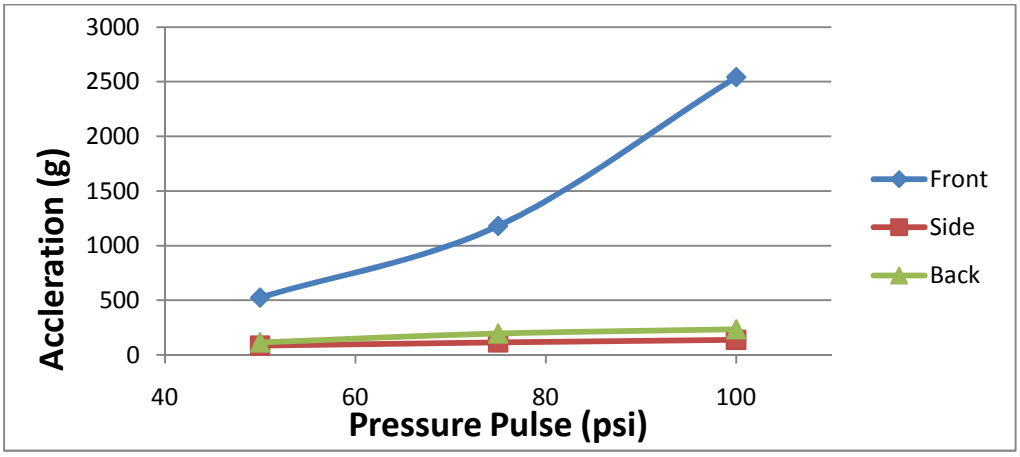

Figure 5-11: Acceleration based on pressure pulses on different spots of the head.

Other than the velocity and acceleration plots, pressure plots were also made. Pressure distribution on the head played a big role in this research. The plot in Figure 5-12 shows the pressure responses on different spots of the head model and the plot in Figure 5-13 shows the pressure difference on the front area of the head model with different pressure pulses.

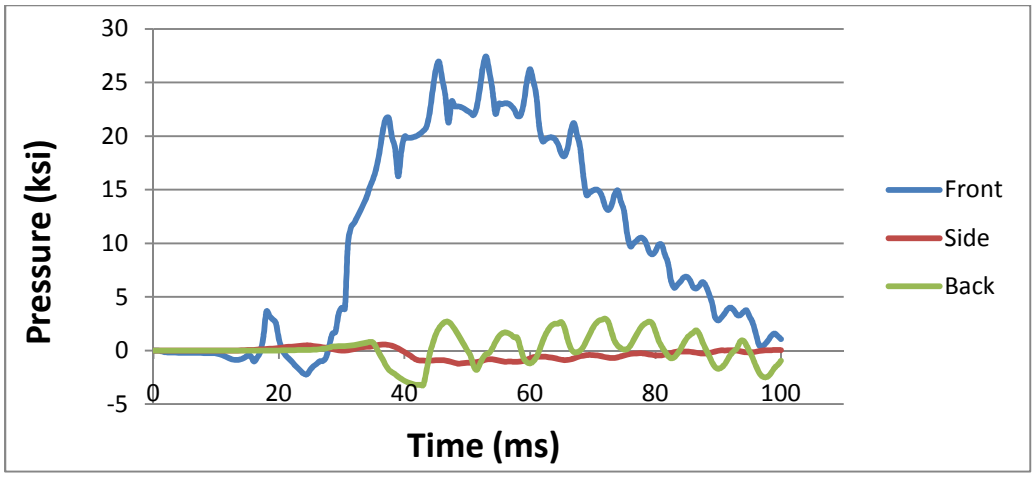

Figure 5-12: Pressure plot with 50 psi pressure pulse on different places of the head model.

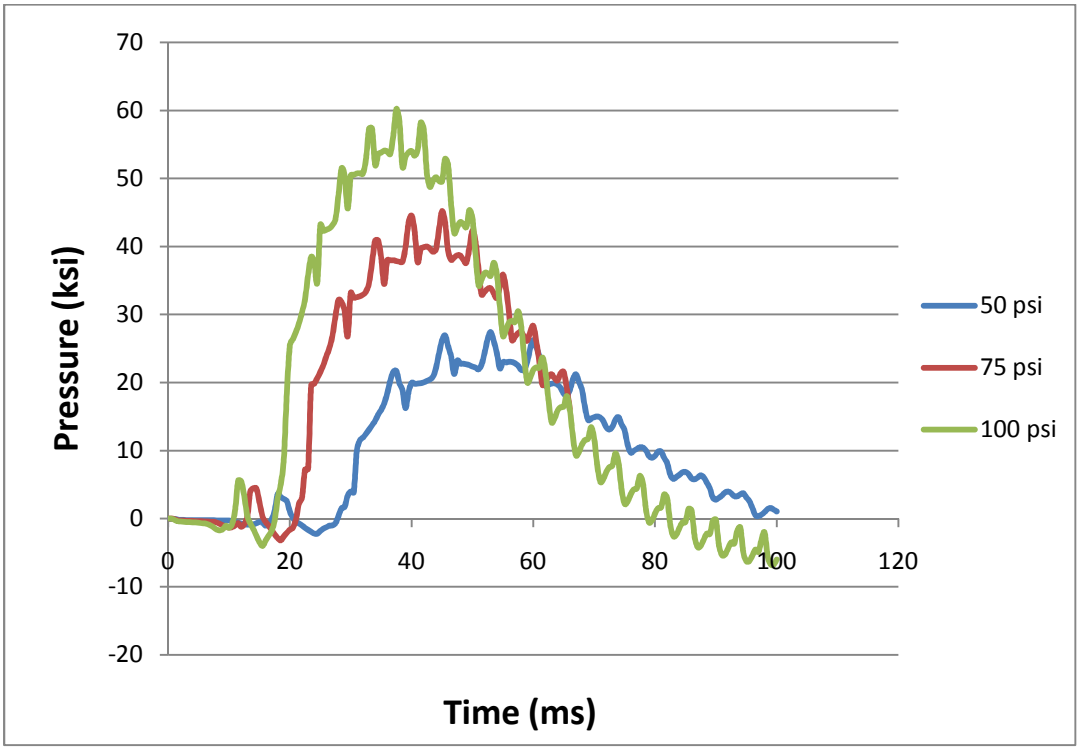

Figure 5-13: Pressure on front area of the head with different pressure pulses.

Similar to the acceleration results, the acceleration on the frontal area of the head model had the greatest values among the three areas, but the pressure

curves were varied from the acceleration curves. The pressure curves would jump up and then back down, forming the positive phase of pressure mentioned earlier.

Figure 5-13 shows that the higher the pressure pulse, the higher the maximum pressure value. Due to the higher pressure pulse, the blast would get to the head model sooner than in the other cases. The 100 psi curve started to react sooner than the 50 and 75 psi curves. The following shows the maximum values on such cases.

	Front	Side	Back
50 psi	27.43 ksi	0.55 ksi	2.99 ksi
75 psi	45.17 ksi	0.86 ksi	3.41 ksi
100 psi	60.24 ksi	1.18 ksi	3.77 ksi

Table 5-4: Maximum pressure based on different pressure pulses on different spots of the head model.

Once again, the maximum values on the frontal area of the head model had some significant differences from the values from the side and back cases. This means that the front of the head experienced the most pressure (which was assumed to be coming from the direction of where the head model is facing) when hit by the blast.

The maximum pressure values were used to plot Figure 5-14, are almost identical to the one showing the maximum values of acceleration in Figure 5-14.

This means that the front surface of the head was affected the most by the change of the pressure pulse.

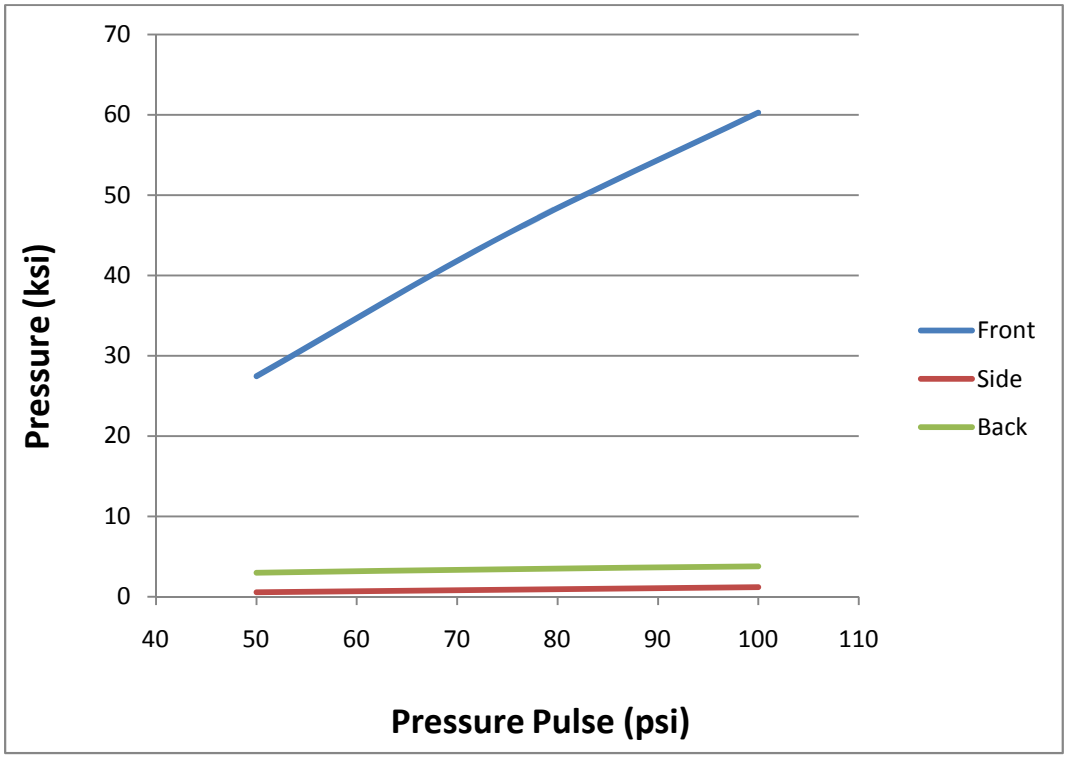

Figure 5-14: Maximum pressure on different spots of the dummy head based on different pressure pulses being used.

5.2. Computational Fluid Dynamics (ANSYS – CFX)

To understand the air flow's reaction over a period of time after the blast was initiated, ANSYS-CFX was used. ANSYS-CFX is a high-performance software that helps solve fluid dynamic problems.

5.2.1. Air Flow Model

The air flow model was first created by using the classic ANSYS program, due to the familiarity of the software and the model was then imported into ANSYS-CFX. Once ANSYS-CFX was used, all the meshing, conditions applying,

and problem solving were completed using this model. Figure 5-15 shows what the model looks like.

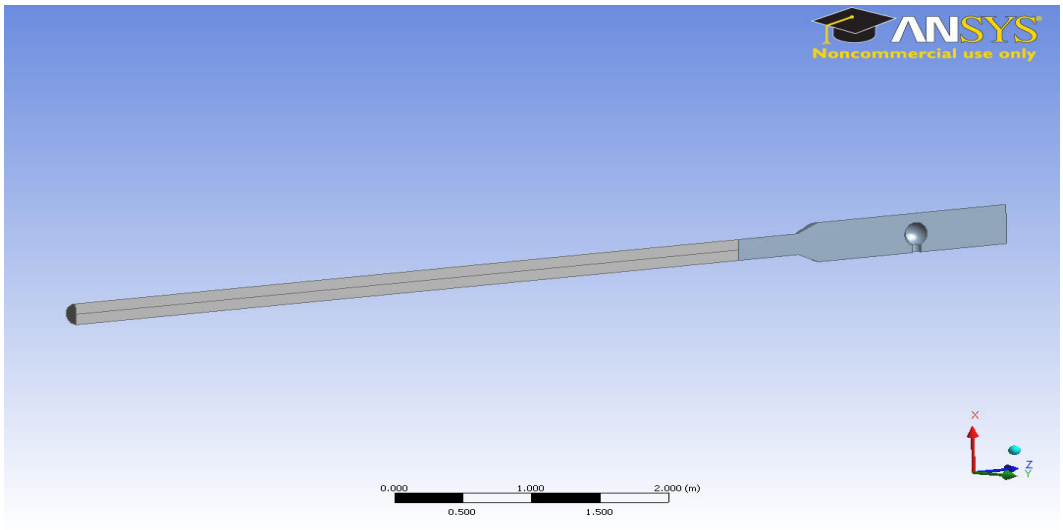

Figure 5-15: Shock tube model used for CFX simulation.

The model was split into two domains which were representing the compressed air inside the driver section pipe and the ambient condition air inside the previously designed chamber pipe. This meant that the domains were separated by the butterfly valve. The head/neck was assumed to be rigid and midway through the chamber pipe. Due to the complication of modeling the Hybrid III dummy head, a simpler model with a combination of a sphere and a cylinder was used for the simulation. That combination of a sphere and cylinder was to be taken out from the chamber domain as mentioned earlier, as the head/neck was assumed to be a rigid body part. The model was also cut in half because the reaction of the air flow at the center point through the pipe could be better shown visually.

5.2.2. Boundary Conditions for the Air Flow Model

There were a few conditions applied to the model. First would be the pressures applied to the two domains of the model. The domain representing the air inside the driver section pipe had an initial pressure of 100 psi, while the other domain representing the normal condition air was set to have an initial pressure of 14.7 psi (the air pressure based on ambient condition). Figure 5-16 shows the model along with the conditions applied.

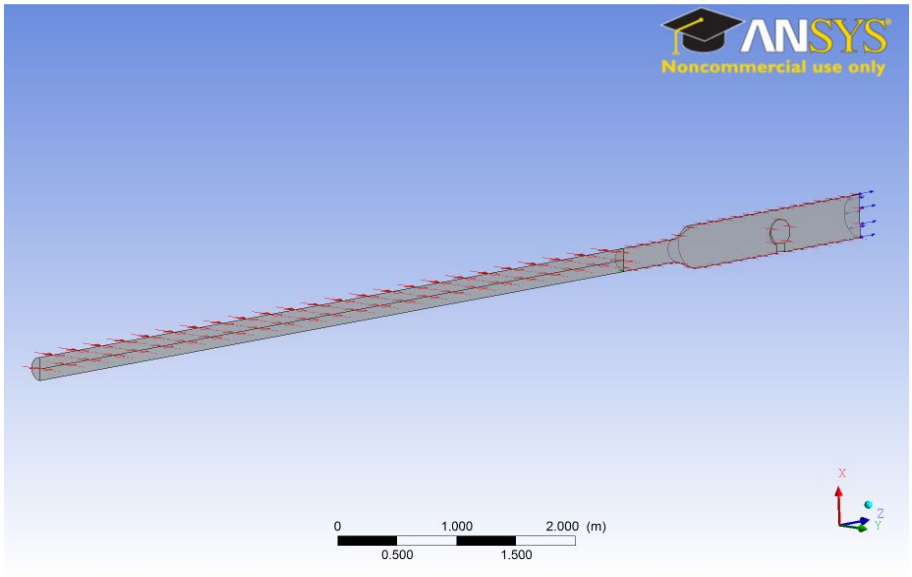

Figure 5-16: Shock tube model along with conditions applied.

Other than the air pressures, the conditions on the outer surfaces were also needed. The most important condition would be the plane that went through the entire model. As the model was being cut in two halves; the symmetric boundary condition was applied to that surface. Next would be the wall conditions for those surfaces that were not supposed to have any movement. Those walls included the closed-end surface (far left in Figure 5-16) and the side surface of

the driver section pipe, the side surface of the chamber pipe, and the surfaces involving the head/neck geometry.

The other end of the chamber air, the side away from the closed-end of the driver section air had an opening boundary condition (far right in Figure 5-16), as that would allow the pressure blast to leave when it got to the end of the air domain instead of bouncing back inside the chamber. As the wall was supposed to be a steel surface, a sand grain roughness of 0.0018 inches was assumed into the simulation setup. Other than that, the interface between the two domains was set to have the default condition. The termination time was to be 20 ms. Finally, the last condition that needed to be applied was the initial condition. In this case, the two air domains were to be set to have initial velocities of zeroes in all three directions because before the air started to move through the shock tube, the air inside the driver section pipe and the chamber pipe were supposed to be stable.

5.2.3. Pressure Distribution inside the Shock Tube

After all the geometry modeling, meshing and conditions applying were complete, the simulation could begin. The transient type simulation usually took a lot longer than running a regular static analysis simulation. That may have been due to the calculation on every single element of the model over a period of time with a specific time step. The plots in Figure 5-17 show the pressure distribution of the air inside the chamber pipe.

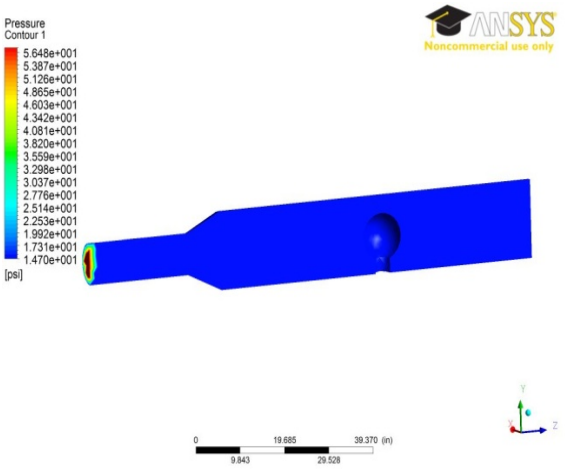
Pressure
Contour 1
5.648e+001
5.387e+001
5.126e+001
4.865e+001
4.603e+001
4.342e+001
4.081e+001
3.820e+001
3.559e+001
3.298e+001
3.037e+001
2.776e+001
2.514e+001
2.253e+001
1.992e+001
1.731e+001
1.470e+001
[psi]
ANSYS
Noncommercial use only
0
19.685
39.370 (in)
9.843
29.528

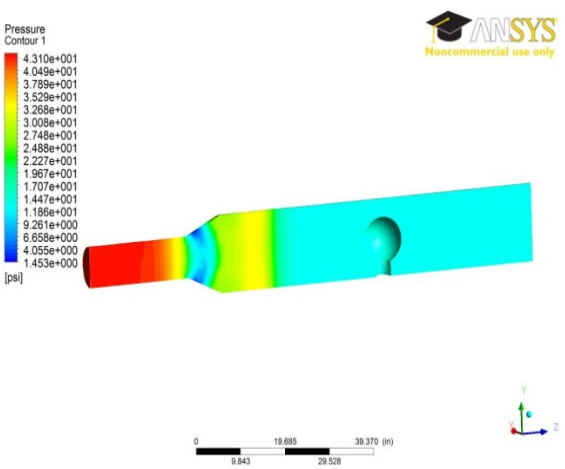
Pressure
Contour 1
4.310e+001
4.049e+001
3.789e+001
3.529e+001
3.268e+001
3.008e+001
2.748e+001
2.488e+001
2.227e+001
1.967e+001
1.707e+001
1.447e+001
1.186e+001
9.261e+000
6.658e+000
4.055e+000
1.453e+000
[psi]
ANSYS
Noncommercial use only
0
19.685
39.370 (in)
9.843
29.528

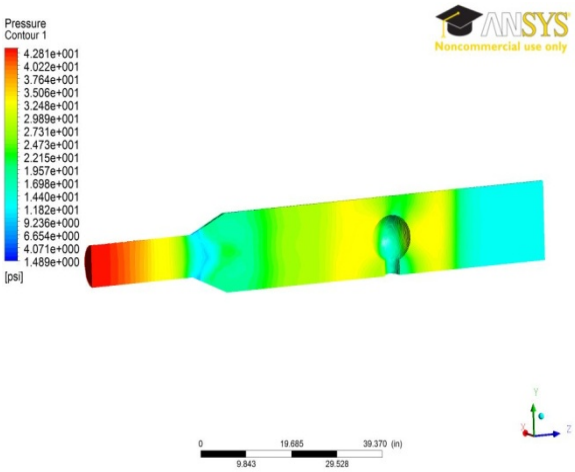
Pressure
Contour 1
4.281e+001
4.022e+001
3.764e+001
3.506e+001
3.248e+001
2.989e+001
2.731e+001
2.473e+001
2.215e+001
1.957e+001
1.698e+001
1.440e+001
1.182e+001
9.236e+000
6.654e+000
4.071e+000
1.489e+000
[psi]
ANSYS
Noncommercial use only
0
19.685
39.370 (in)
9.843
29.528

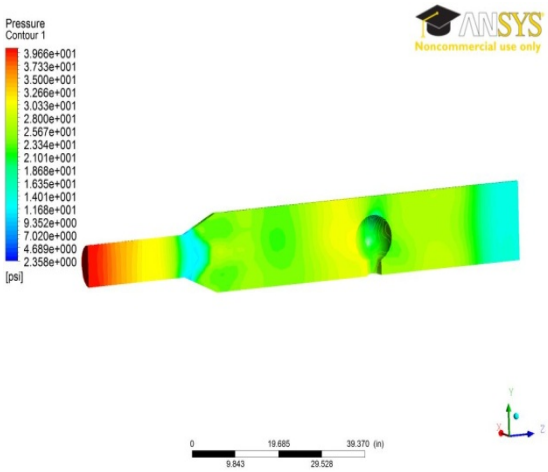
Pressure
Contour 1
3.966e+001
3.733e+001
3.500e+001
3.266e+001
3.033e+001
2.800e+001
2.567e+001
2.334e+001
2.101e+001
1.868e+001
1.635e+001
1.401e+001
1.168e+001
9.352e+000
7.020e+000
4.689e+000
2.358e+000
[psi]
ANSYS
Noncommercial use only
0
19.685
39.370 (in)
9.843
29.528

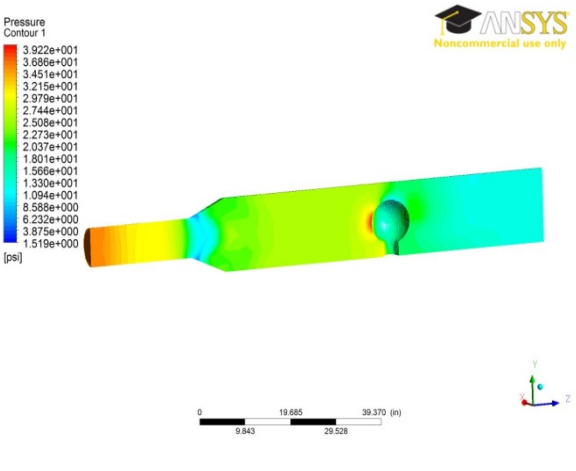
Pressure
Contour 1
3.922e+001
3.686e+001
3.451e+001
3.215e+001
2.979e+001
2.744e+001
2.508e+001
2.273e+001
2.037e+001
1.801e+001
1.566e+001
1.330e+001
1.094e+001
8.588e+000
6.232e+000
3.875e+000
1.519e+000
[psi]
ANSYS
Noncommercial use only
0
19.685
39.370 (in)
9.843
29.528

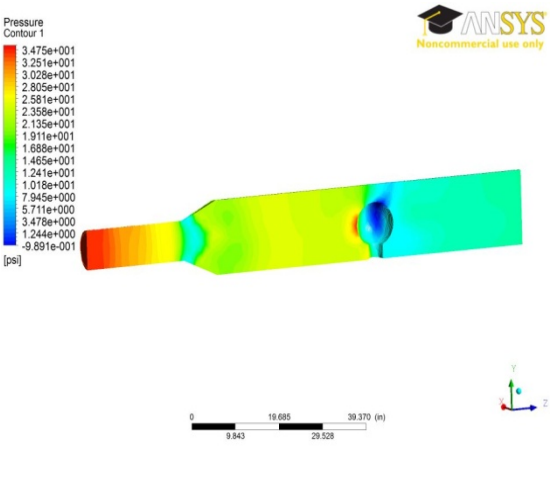
Pressure
Contour 1
3.475e+001
3.251e+001
3.028e+001
2.805e+001
2.581e+001
2.358e+001
2.135e+001
1.911e+001
1.688e+001
1.465e+001
1.241e+001
1.018e+001
7.945e+000
5.711e+000
3.478e+000
1.244e+000
-9.891e-001
[psi]
ANSYS
Noncommercial use only
0
19.685
39.370 (in)
9.843
29.528

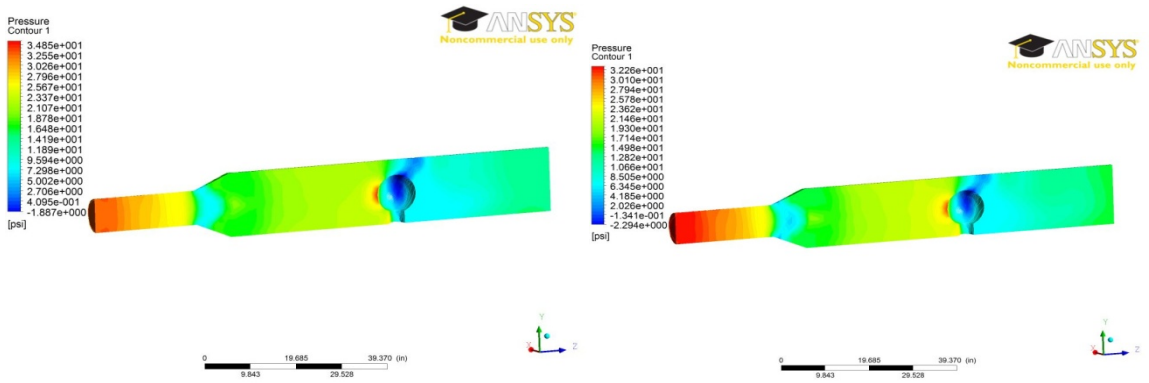

Figure 5-17: Pressure distributions at t = a) 0, b) 3, c) 6, d) 9, e) 12, f) 15, g) 18, h) 20 ms.

At the initial stage (Figure 5-17a), air inside the chamber pipe (dark blue in Figure 5-17a) was stable because an initial pressure of 14.7 psi was applied. When the time reached 3 ms (Figure 5-17b), the shock wave of blast got into the chamber pipe (yellow and lime in Figure 5-17b). There is a dark blue section right where the cross-sectional area is increased because when the air was pushed faster than the speed of sound, a space of vacuum occurred and that created the negative phase of the blast.

Figures 5-17c) and 5-17d) show that the blast got past the head/neck and the blast reached the open-end of the chamber pipe. At the other end, it is red because the high pressure was still coming out from the driver section pipe, but the maximum pressure at the red section dropped from the initial pressure of 100 psi to 39.66 psi.

The next stage shows the negative pressure was still at the flow expander, with a pressure of 1.519 psi while the initial pressure was set to be 14.7 psi. One difference from the previous figures occurred in the front of the head where high

pressure was created with a pressure of 39.22 psi, as the high speed flow was being slowed down by the head.

The next three plots (Figures 5-17 e f g) are extremely similar in that the maximum pressure occurred where the compressed air was being released or in front of the head. The minimum pressure section was moved from the flow expander to somewhere behind the head, and it was getting lower over time. In Figure 5-17e, the minimum pressure dropped to -0.989 psi, and in Figure 5-17g, it kept going down to -2.294 psi. Other than the pressure distribution animation, pressure or velocity at any point in the system can also be shown. The following plots (Figure 5-18) show the velocity and pressure curves at a few specific points in the system so different reactions can be seen.

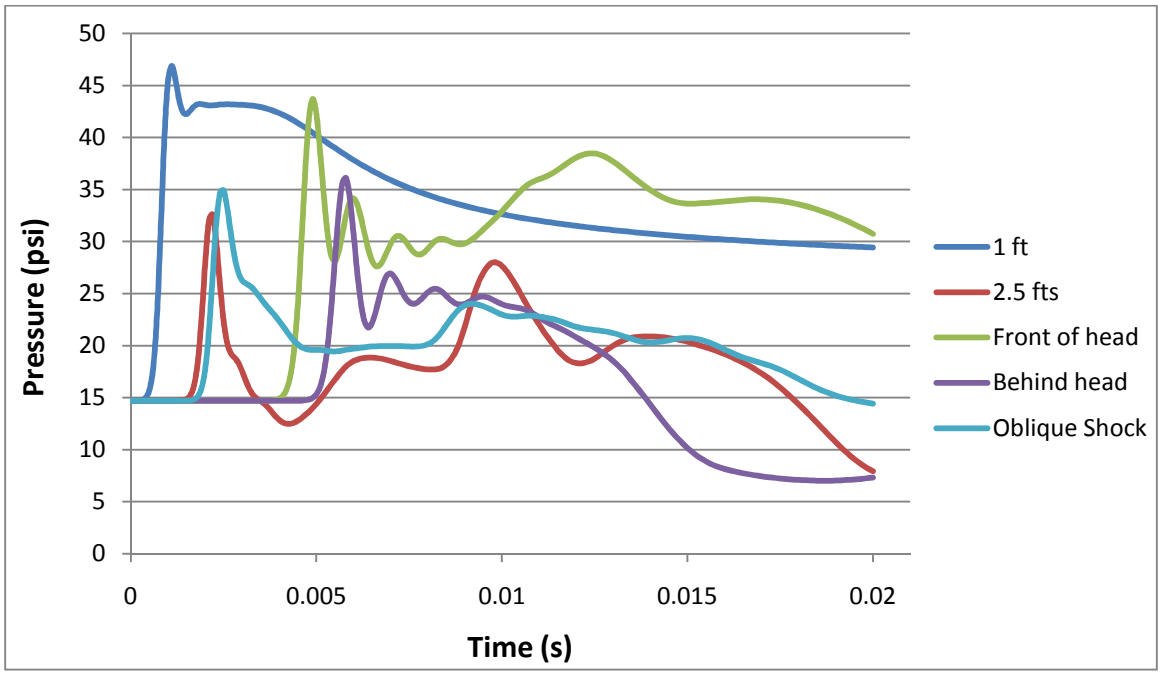

Figure 5-18: Pressure vs. Time plot at 5 different spots in the system.

The first point selected for the plot was one foot away from the butterfly valve at the center point of the circular flow. As shown, the pressure increased to

roughly 47 psi from 14.7 psi in 1.1 ms, due to the rapid air flow going through the point. Then the pressure decreased slowly as the compressed air coming out from the driver section pipe was getting less pressure, it decreased to 29.43 psi at t=20ms, but, in time, will likely return to ambient pressure.

The second point selected was 2.5 feet away from the butterfly valve. The curve shows that there was a pressure jump at about t=2.5 ms. The pressure then dropped below 14.7 psi, meaning that the negative pressure was created due to the high speed of air flow.

The other three points selected were at the front of the head, behind the head, and at the end of the flow expander. In the case of in front of the head, the pressure simply increased when the blast reached the front of the head. The pressure then decreased some but increased again as the second wave of blast approached.

Figure 5-19 shows the velocity plot at different points in the system over a time period of 20 ms, which is the same as the ones selected for the previous plot. The first one was one foot away from the butterfly valve and the curve shows a jump of velocity at about 1 ms and then it went up slowly. The curve went up slowly because the point was so close to the valve, keeping the air flow stable enough to have such distribution. The point that was 2.5 feet away from the valve had a velocity distribution that is shown as the red curve. It first went up due to the blast, and then the curve continued to go up rapidly until it got to about 1200 ft/s and then the velocity remained at that range 5 ms after the blast began. The second increase of velocity on the second point was supposed to be due to

the Prandtl-Meyer expansion fan process, meaning that when the air flow was having a speed over the speed of sound and reaching to an increase of the cross-sectional area of the testing pipe, the velocity of the air flow would increase.

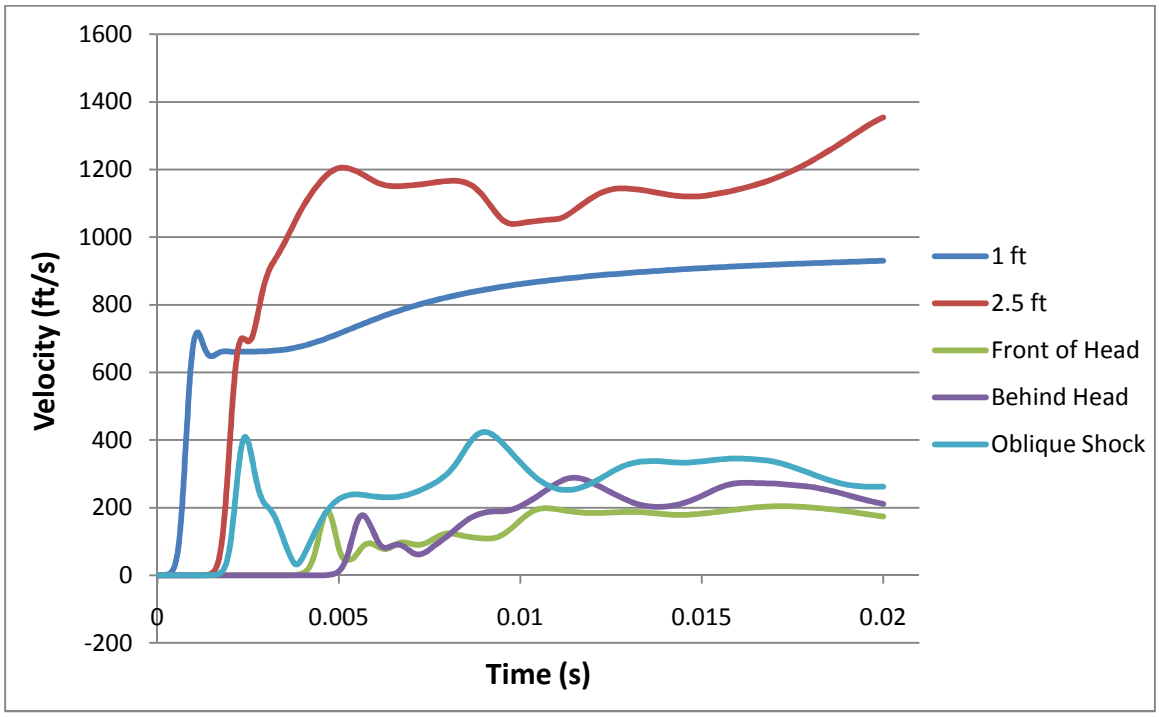

Figure 5-19: Velocity vs. time plot at five different spots in the system.

The velocity curves for the other three points were relatively small compared to the other two points mentioned earlier. This was due to the flow hitting on the head and the flow being limited by the oblique shock. The air flow in the chamber pipe had a maximum velocity of roughly 1900 ft/s (about Mach 1.7) at where the cross-sectional area started getting larger. This was also due to the Prandtl-Meyer expansion fan process.

CHAPTER 6. CONCLUSIONS

In this thesis, experimental and numerical approaches were used to determine the linear velocity, acceleration, and pressure of the Hybrid III dummy head when it is hit by shock waves from a blast. For the experimental approach, a blast shock tube was built for the laboratory settings. For the numerical approach, a simple elastic FE head/neck model was used for the dynamic simulation. The relationships between the pressure pulse and the linear acceleration/velocity and the standoff distance were found.

The following are some conclusions made based on the results obtained from the experiments:

1. When the operating pressure pulse is increased proportionally, the maximum velocity and acceleration of the head/neck increase exponentially when sliding through the rails.
2. As the operating pressure pulse is set to be higher, the instability on the velocity curves increases. When 50 psi pressure pulse is used, the velocity curve is more linear than the ones for the 50 and100 psi pressure pulses; and that would be due to the bending movement of the head/neck, rippling of the rubber face, and the friction caused by the rails.
3. When the dummy head is placed at a specific standoff distance, it shows that when the operating pressure pulse gets higher, the difference between the maximum velocity values gets larger.

4. Similar to the results for the maximum velocities, it shows that when the operating pressure pulse gets higher, the difference between the maximum acceleration values also gets larger.
5. From the results obtained by using accelerometers, it is shown that the accelerations would go down when lowering the setup pressure pulse, or when placing the dummy head further away from the shock tube opening, but with some unexpected results at the same time. The unexpected results could be due to the inaccuracy of accelerometers setup, the inaccuracy of the accelerometers readings, the instability of the air flow, noise, or the vibrations of the dummy head caused by the blast.

In another part of the research, a simple elastic model was used for FEA focusing on the air flow and the dummy head. This is mainly based on the reactions of the head/neck model.

1. When the FE model has a valve involved, it shows that when the head/neck model is placed 5 inches away from the shock tube opening, the velocity of the head/neck is much higher than the ones when the head model is placed 7.5 and 10 inches away from the shock tube opening. That would be due to the instability of the flow caused by the turning valve.
2. As the model including the valve had some unexpected results, a few more simulations were done with the same model, but with the valve part removed. In this case, the results are showed two facts: 1) when the head is set to be at the same placement for all the simulations, the higher the pressure pulse is set, the higher the velocity, acceleration, and pressure is

on the head model, and 2) the frontal area of the head model is always having the highest pressure among the three different spots of the head model including the frontal, side, and back surfaces of the head model.

The last part of the research is also involved the FEA, but it is concentrated on the air flow inside the pre-designed testing chamber instead of on the velocity and acceleration of the Hybrid III dummy head.

The following are some conclusions made based on the results obtained from the analyses:

1. Two different pressures were applied to the two air domains in the model. One had a pressure of 100 psi while the other has a pressure of 14.7 psi. Although there was only an interface separating the two domains, the maximum pressure of the air inside the chamber pipe increased instantly to roughly 56.5 psi.
2. Within the 20 ms time period of simulation, the value of maximum pressure dropped slowly, and the place of the maximum pressure kept changing between the butterfly valve and the front of the head.
3. The maximum velocity of the air flow occurred at the flow expander, as the direction of the air flow became more unidirectional before the air went to the flow expander section. The air flow in the same section had a higher velocity than the other sections of the chamber pipe as well. This was due to the Prandtl-Meyer expansion fan process. Assuming the speed of sound is 1126 ft/s, the maximum velocity of the flow there was found to be

roughly 1622 ft/s, which turned out to have a Mach number of 1.44, meaning that the air flow reached the level of supersonic.

4. Negative pressure (lower than 14.7 psi) happened at two spots when the compressed air flowed through the chamber. One was at the beginning of the flow expander and the other was at the backside of the head. The negative pressure happened because of the high speed of the air flow but it does not last for long.

CHAPTER 7. RECOMMENDATIONS FOR FUTURE STUDIES

The following are some recommendations for the research in the future:

1. The chamber pipe was extremely heavy and it would be more convenient if it had been lighter. The unused chamber pipe, along with the flow expander weighed a few hundred pounds, and it was, therefore, very difficult to move; it was also connected to a stand had to be moved up and down. It would be possible to find a six feet long acrylic chamber pipe with a thickness of half an inch. Once the transparent chamber pipe was used for the experimental setup, the reaction of the Hybrid III dummy head could be captured by a high speed camera which would be easier and safer.
2. There was an extremely small leakage of pressure coming out from the butterfly valve. Results would be more accurate if the leakage problem was repaired. The shock tube designed for this research used a pneumatic actuator along with a solenoid and a butterfly valve. The minor loss of pressure from the butterfly valve may have affected the experimental results and the results could perhaps be improved if the butterfly valve was replaced by using a diaphragm.
3. More components such as more pressure sensors or flow velocity transducers at different spots inside the chamber pipe could be added to

the laboratory settings. This would help with understanding the pressure and velocity distributions of the air flow for the specific shock tube.

4. There may have been more errors due to the size and turning time (it took about 0.5 seconds when no compressed air was inside the driver section pipe) of the butterfly valve, as it may have caused a significant loss of pressure. The design of the shock tube may need to be changed to use a membrane instead of the butterfly valve.
5. For the FEA part of the research, a more accurate model is needed. The FE model of the Hybrid III dummy head includes the rubber and metal part of the head and neck, meaning that the head/neck model would have different mechanical properties. Having a ballistic helmet model would help in understanding the usage/effect of a ballistic helmet and could be beneficial in understanding the entire blast model.

REFERENCES CITED

Anderson, R.J. (2008). Shell Shock: An Old Injury with New Weapons. *Molecular Interventions, 8,* 204-218.

Boyer, D.W. (1960). An experimental study of the explosion generated by a pressurized sphere. *Journal of Fluid Mechanics, 9*. 401-29.

Brooks, A. J., Clasper, J., Midwinter, M. J., Hodgetts, T. J., & Mahoney, P. F., *Ryan's Ballistic Trauma: A Practical Guide*, New York: Springer, 1997. Print.

CFX. (2012). Computer Software. Canonsburg, PA: ANSYS.

Chafi, M.S., Dirisala, V., Karami, G., & Ziejewski, M. (2010). A FE parametric study of the dynamic response of the human brain with different CSF constitutive properties. *Bio-Medical Materials and Engineering.* DOI 10.3233/BME-2010-0619.

Chafi, M.S., Karami, G., & Ziejewski, M., (2010). Biomechanical Assessment of Brain Dynamic Responses Due to Blast Pressure Waves. *Annals of Biomedical Engineering, 38*. 490-504.

Chafi, M.S., Karami, G., & Ziejewski, M. (2009). Numerical analysis of blast-induced wave propagation using FSI and ALE multi-material formulations. *International Journal of Impact Engineering, 36*. 1269-1275.

Helmick et al. (2006). Defense and Veterans Brain Injury Center Working Group on the Acute Management of Mild Traumatic Brain Injury (mTBI) in Military Operational Settings. *Clicical Practice Guideline and Recommendations.* Washington, DC: Defense and Veterans Brain Injury Center.

Cifu et al. (2009). Defense and Veterans Brain Injury Center Consensus Conference. Acute Management of Concussion/mild Traumatic Brain Injury (mTBI) in the Deployed Setting. Washington, DC: Defense and Veterans Brain Injury Center.

Dirisala, V., Karami, G., & Ziejewski, M. (2011). Effects of neck damping properties on brain response underimpact loading. *International Journal for Numerical Methods in Biomedical Engineering*. DOI: 10.1002/cnm. 1480.

Dobratz, B.M., & Crawford, P.C. (1985). LLNL Explosives Handbook, Properties of Chemical Explosives and Explosives Stimulants; UCRL-52997; Lawrence Livermore Laboratory: Livermore CA.

Finkelstein, E., Corso, P., & Miller, T. (2006). The Incidence and Economic Burden of Injuries in the United States. New York (NY): Oxford University Press.

Gibson, P. (1994). Blast overpressure and survivability calculations for various sizes of explosive charges. *Technical Report. Army Natick Research Development and Engineering Center MA*.

Glasser, R.J. (2007, April). A Shock Wave of Brain Injuries. Retrieved from http://dva.state.wi.us/Docs/TBI/A_ShockWave_of_Brain_Injuries.pdf

HyperMesh Computer Software. Troy, MI: Altair Engineering. (2012).

Karami, G., Grundman, N., Abolfathi, N., Naik, A., & Ziejewski, M. (2009). A micromechanical hyperelastic modeling of brain white matter under large deformation. *Journal of the Mechanical Behavior of Biomedical Materials, 2*. 243-254.

Kinney, G.F., Graham, K.K. (1985). Explosive Shocks in Air. Springer-Verlag New York Inc., New York.

LabView (Version 8.6) Computer Softwar]. Austin, TX: National Instruments. (2012).

Leonardi, A. D. C., Bir, C. A., Ritzel, D. V., & VandeVord, P. J. (2011, January). Intracranial Pressure Increases during Exposure to a Shock Wave. *Journal of Neurotrauma, 28,* 85-94.

LS-DYNA (Version 971) Computer Software. Livermore, CA: Livermore Software Technology Corporation. (2012).

Magnuson, S. (2010). Scientists Hope Bomb Blast Research Can Lead to Better Helmets. *National Defense, 95*.

Management of Concussion/mTBI Working Group. (2009). VA/DoD Clinical Practice Guideline for Management of Concussion/mild Traumatic Brain Injury: VA/DoD Evidence Based Practice. Washington, DC: Department of Veterans Affairs.

Nahum, A.M., Smith, R., & Ward, C.C. (1977). Intracranial pressure dynamics during head impact. *Proceedings of the 21st Stapp Car Crash Conference,* 339-366。

Segars. R. A., & Carboni, M. G. (2008). A Shock Tube for Downselecting Material Concepts for Blast Protection Part I: Description of the Shock Tube and a Comparison of Flush Mounted and Recess Mounted Pressure Sensors. *U.S. Army Natick Soldier Research, Development and Engineering Center*.

Sharma, S., & Zhang, L. (2011). Prediction Of Intracranial Responses from Blast Induced Neurotrauma using a Validated Finite Element Model of Human Head.

Tan, P., Lee, B., & Tsangalis, C. (2010). Finite element analysis of sandwich panels subjected to shock tube blast loadings. *Journal of Sandwich Structures and Materials OnlineFirst*, 1-16.

Tanielian, T., Jaycox, L. H. (EDS.) (2008). Invisible Wounds of War: Psychological and Cognitive Injuries, their Consequences, and Services to Assist Recovery. Santa Monica, CA: RAND Center for Military Health Policy Research.

Varas, J. M., Philippens, M., Meijer, S. R., van den Berg, A. C., Sibma, P. C., van Bree, J. L. M. J., & de Vries, D. V. W. M. (2012). Physics of IED Blast Shock Tube Simulations for mTBI Research. *Frontiers in Neurology*. V.2.

WebRef1: Brain Injuries and Mass Casualty Events. (2005). Retrieved from http://emergency.cdc.gov/masscasualties/braininjuriespro.asp

WebRef2: Explosions and Blast Injuries: A Primer for Clinicians. (2012). Retrieved from http://emergency.cdc.gov/masscasualties/braininjuriespro.asp

WebRef3: Explosives. (2011). Retrieved from http://www.globalsecurity.org/military/systems/munitions/explosives.htm

WebRef4: Traumatic Brain Injury. (2012). Retrieved from www.ninds.nih.gov/disorders/tbi/tbi.htm

Ziejewski, M., Karami, G., & Akhatov, I. (2007). Selected Biomechanical Issues of Brain Injury Caused by Blasts. *Brain Injury/professional*, vol. 4 issue 1.